

## Dusty Disks around White Dwarfs I: Origin of Debris Disks

Ruobing Dong<sup>1,2\*</sup>, Yan Wang<sup>1,3</sup>, D. N.C. Lin<sup>1,4</sup>, and X.-W. Liu<sup>1,5</sup>

<sup>1</sup>*Kavli Institute of Astronomy and Astrophysics, Peking University, Beijing, China*

<sup>2</sup>*Department of Astrophysical Sciences, Princeton University, Princeton, NJ 08544, USA;  
rdong@astro.princeton.edu*

<sup>3</sup>*Department of Astronomy and Astrophysics, Penn State University, State College, PA 16802,  
USA; yuw123@psu.edu*

<sup>4</sup>*Department of Astronomy and Astrophysics, University of California, Santa Cruz, CA 95064,  
USA; lin@ucolick.org*

<sup>5</sup>*Department of Astronomy, Peking University, Beijing China; liuxw@bac.pku.edu.cn*

### ABSTRACT

A significant fraction of the mature FGK stars have cool dusty disks at least an orders of magnitudes brighter than the solar system's outer zodiacal light. Since such dusts must be continually replenished, they are generally assumed to be the collisional fragments of residual planetesimals analogous to the Kuiper Belt objects. At least 10% of solar type stars also bear gas giant planets. The fraction of stars with known gas giants or detectable debris disks (or both) appears to increase with the stellar mass. Here, we examine the dynamical evolution of systems of long-period gas giant planets and residual planetesimals as their host stars evolve off the main sequence, lose mass, and form planetary nebula around remnant white dwarf cores. The orbits of distant gas giant planets and super-km-size planetesimals expand adiabatically. During the most intense AGB mass loss phase, sub-meter-size particles migrate toward their host stars due to the strong hydrodynamical drag by the intense stellar wind. Along their migration paths, gas giant planets capture and sweep up sub-km-size planetesimals onto their mean-motion resonances. These planetesimals also acquire modest eccentricities which are determined by the mass of the perturbing planets, the rate and speed of stellar mass loss. The swept-up planetesimals undergo disruptive collisions which lead to the production of grains with an extended size range. The radiation drag on these particles is ineffective against the planets' resonant barrier and they form 30-to-150-AU-sizes rings which can effectively reprocess the stellar irradiation in the form of FIR

---

\*Correspondence should be addressed to rdong@astro.princeton.edu.

continuum. We identify the recently discovered dust ring around the white dwarf WD 2226-210 at the center of the Helix nebula as a prototype of such disks and suggest such rings may be common.

*Subject headings:* stars: AGB and post-AGB — stars: evolution — (ISM:) planetary nebulae: general — stars: individual (WD2226-210) — (stars:) planetary systems — methods: numerical

## 1. Introduction

The discovery of over 300 planets shows that at least 10 % of nearby solar type stars have Jupiter-mass planets around them (Cumming *et al.* 2008). According to widely adopted sequential accretion hypothesis, these planets formed through condensation of heavy elements, emergence of planetesimals which coagulated into protoplanetary embryos and cores prior to efficient gas accretion. Through a series of population-synthesis simulations based on this scenario (Ida & Lin 2004a,b, 2005, 2008a,b), we were able to reproduce the observed mass-period ( $M_p - P$ ) distribution of the known gas giant planets (Schlaufman *et al.* 2008) around a modest fraction ( $\eta_J$ ) of FGK main sequence dwarf stars.

Mass accretion rate  $\dot{M}$  from protostellar disks onto stars more massive than the Sun is observed to increase with square of the stellar mass *i.e.*  $M_*^2$  (Natta *et al.* 2006, Garcia-Lopez *et al.* 2006, cf Clarke & Pringle 2006). If the initial mass of these disks also increases with  $M_*$ , the greater availability of heavy elements would provide more rapid growth and larger of protoplanetary embryos around intermediate mass stars (Ida & Lin 2004b, 2005, Kennedy *et al.* 2007). Furthermore, the extended local surface density and pressure maxima at the ionization radius (where the mid-plane temperature  $T_c \simeq 1000$  K), snow line (Kretke *et al.* 2009), and outer edge of the dead zone provide more efficient barrier against hydrodynamic drag for the sub-km grains and type-I migration for the critical-mass ( $\sim 10M_\oplus$ ) cores. The enhance retention efficiency of these building blocks enhance emergence probability of gas giants (Laughlin *et al.* 2004, Ida & Lin 2004b).

On the observational side, high-precision radial-velocity surveys of intermediate-mass main sequence stars have been handicapped by their hot and active atmosphere as well as their fast spin (Griffin *et al.* 2000). However, these problems are significantly reduced when these stars evolve off their main sequence. Several planets have been found around G sub-giants and giants (Sato *et al.* 2005) which have more expanded envelopes and relatively cool atmospheres. Preliminary surveys indicate that the fraction of these relatively massive G giant stars with gas giant planets ( $\eta_J \sim 1/3$ ) may be more than double that around the solar-type G dwarf main sequence stars (Sato

*et al.* 2007, Johnson *et al.* 2007, Dollinger *et al.* 2007, Hatzes 2008, Johnaon 1008).

Another area where observations provide valuable clues on the planet formation process is the search for residual building-block planetesimals around their host stars. Since 1995 a population of Kuiper Belt objects (KBO's) has been found in the solar system and beyond the orbit of Neptune (Jewitt & Luu 1995, Brown *et al.* 2005). These objects are thought to be the parent bodies of a diffuse dusty ring which emits cold zodiacal light with far infrared (FIR) radiation.

A series of recent systematic  $70 \mu\text{m}$  (FIR) observational surveys with the Spitzer Infrared Space Telescope indicate that 1) none of the nearby M stars show detectable excess (Gautier *et al.* 2007), 2) 15 % of 274 FGK stars show excess (Bryden *et al.* 2006, Beichman *et al.* 2006, Trilling *et al.* 2008), 3) 30 % of 160 A stars also show excess (Rieke *et al.* 2005; Su & Rieke 2007). The threshold level for a marginal detection by the Spitzer Telescope is at least an order of magnitude more intense that of the solar system zodiacal light.

Since both the fraction of stars with gas giants ( $\eta_J$ ) and that with detectable debris disks ( $\eta_d$ ) increases with the stellar mass ( $M_*$ ), we can extrapolate that a major fraction of intermediate-mass stars may have both gas giants and persistent, rich debris disks. This inferred association of gas giant planets with debris disks is highlighted by the recent discovery (with adaptive imaging technique) of three gas giants and a debris disk outside them around an A5V star HR 8799 (Marois *et al.* 2008). The mass and periods of these three planets are (10, 10, 7)  $M_J$  and (24, 38, 68) AU. Around this  $M_* = 1.5M_\odot$  star, the ice line is located at  $\sim 10$  AU. In §2, we provide a more detailed discussion on the association of debris disks and planet formation in the Solar System and around nearby stars.

With the evidence of existence of many detectable debris disks and gas giant planets around nearby, mature, intermediate-mass stars, we now consider their dynamical evolution during the post main sequence evolution of their host stars. The goal of our study here is to identify whether the inconspicuous planet building blocks may reveal their presence. The analysis to be presented below is particularly relevant for the AGB mass loss phase where the mass loss rates range up to  $\sim 10^{-4}M_\odot \text{ yr}^{-1}$  and where most of the stars may reach this mass loss rate near the end of the AGB phase (Willson 2000). The typical outflow speed is  $\sim 10 \text{ km s}^{-1}$  and  $\dot{M}_*$  may vary on the time scale of  $10^{3-4} \text{ yr}$  (Weidemann 1987, Blocker 1997). After losing mass on the AGB, these stars rapidly evolve across the HR diagram to form planetary nebula around emerging white dwarfs. During the post AGB phase, although high-speed mass loss continue to occur, the mass flux is much reduced (cf Kwok 1982).

In this paper, we mostly consider stars with a main-sequence masses in the range of  $2M_\odot < M_* < 4M_\odot$  (A-F stars). We choose these stars not only because many, perhaps most of them, have gas giants and debris disks (similar to those around the less massive Sun and HR 8799), but they are

also thought to be the progenitors of some well known planetary nebulae such as the Helix nebula where the mass of the remnant white dwarf WD 2226-210 is  $\sim 0.58M_{\odot}$  (Su *et al.* 2007). This rapid and large-magnitude change in the gravitational potential can lead to great orbital expansions for their planets. This evolutionary tendency may lead to the possibility of resolvable HST imaging of long-period planets which are otherwise undetectable.

Evidence for the existence of residual planetesimals comes from the recent discovery of a dusty ring around a young white dwarf WD 2226-210 at the center of the Helix nebula (Su *et al.* 2007). This ring extends between about 35 and 150 AU from a central white dwarf WD 2226-210 (well interior to the complex, helix structure), and have a total mass of about  $0.13 M_{\oplus}$ . We propose that this ring is the byproduct of planets and planetesimals' orbital evolution during the epoch when the central star rapidly lost most of its mass. Based on the extrapolation of the system around HR 8799, our basic conjectures are:

- 1) gas giant planets and debris disks are common around A main sequence stars;
- 2) at the epoch of their main sequence turnoff, these relatively massive stars have debris disks with more than  $10M_{\oplus}$  in total mass and most of it is contained in km-size residual planetesimals
- 3) gas giant planets' orbits expanded adiabatically by nearly an order of magnitude while there host stars evolve through AGB mass loss phase with rapid stellar mass loss;
- 4) the KBO-equivalent planetesimals are captured onto the main motion resonance of gas giants; and
- 5) through collisions, these parent bodies generate dust which reprocess the radiation of their central star.

These basic assumptions are based on their solar system and HR 8799 analogues. A detailed and systematic analysis of these processes is useful for understanding the long-term evolution of this class of planetary systems. In §3, we first construct a working model for a solar-system like configuration. The orbital evolution of the planets and planetesimals is computed and analyzed in §4. Here we take into account of the central star's mass loss, the hydrodynamic drag by the expanding envelope and the planet's dynamical perturbation on the residual planetesimals. In §5, we show that collisions between the resonant planetesimals lead to their disruptions and fragmentation. We derive the condition for the retention of dust grains into rings outside the orbits of some gas giant planets. We model the structure of the disk around WD 2226-210 in §6. Finally, we summarize our results and discuss their implication, especially in the context of possible detectable gas giant planets around young white dwarfs in §7.

## 2. Association of debris disks and gas giants

In this section, we briefly recapitulate existing observational information on the inventory of residual planetesimals in the outer solar system and around mature, intermediate-mass main-sequence stars. These data will be used in the subsequent sections for the development of our working model.

### 2.1. Inventory of residual KBO's in the outer solar system.

KBO's are marginally preserved at their remote location because planetary perturbation (by gas and ice giants) is relatively weak (Duncan & Quinn 1993). However, their present-day spatial distribution also poses a challenge to the formation of the largest KBO's which have masses comparable to Pluto. If their building blocks were initially smoothly distributed with respect to their distances from the Sun, *in situ* formation of such large KBO's would require more than a few  $M_{\oplus}$  of planetesimals in the region 30-50 AUs (Stern 1996, Youdin & Chiang 2004). This required total mass is  $\sim 2$  orders of magnitude larger than the total reservoir of all known KBO's. Dynamical perturbation by Uranus and Neptune can induce a substantial depletion from a massive initial inventory to the present-day KBO reservoir (Duncan & Quinn 1993). This stringent requirement would be relaxed under the assumption that the most massive KBO's were formed closer to the Sun and then scattered to their present-day location by gas or ice giant planets either during the advanced phase of their formation (Zhou & Lin 2007) or through long term dynamical evolution of the system (Duncan *et al.* 1987).

It is possible that the size distribution of the KBO's extend well below the present detection limit. Elsewhere in the solar system, the crater density on the unprocessed moons of the outer planets (Hartmann 1999) indicate that they have been bombarded by meteorites with a size distribution  $dN/ds \propto s^{-3.5}$  as observed among the asteroids (Gradie *et al.* 1989). This distribution is probably the byproducts of a collisional equilibrium (Donanyi 1969, Williams & Wetherill 1994, Farinella & Davis 1996, Tanaka & Ida 1996, Kenyon & Bromley 2002, Weidenschilling 2004). On the small-size limit, particles in Saturn's rings (Cuzzi *et al.* 1980) and grains in the interstellar medium (Mathis *et al.* 1977, Laor & Draine 1993) follow a similar pattern. With such a size distribution, most of the surface area is covered by the small particles while a large fraction of the total mass is contained in the large particles.

As a population, the KBO's have a directly-observed size distribution  $dN/ds \propto s^{-5}$  for  $s > 100\text{km}$  (Trujillo *et al.* 2001) whereas, below  $s \sim 70\text{ km}$ ,  $dN/ds$  is considerably shallower than  $s^{-3.5}$ , (*i.e.* there is a deficit of small particles) down to the detection limit of a few 10 km (Bernstein *et al.* 2004). This break in the slope of the size distribution implies a large fraction of the KBO's

total mass is contained in particles with  $s \sim 10 - 100$  km. One possible reason for this complex power-law distribution is the collisional fragmentation of KBO's as piles of loose gravels (Pen & Sari 2005).

At their present distance, it is difficult to directly image planetesimals smaller than a few 10km. However, micron to sub-mm particles in the asteroid belt and Kuiper belt scatter and reprocess the solar radiation to produce warm and cold zodiacal light (Backman *et al.* 1995). Due to the Poynting-Robertson (PR) drag induced on them by the stellar photons, the grains undergo orbital decay on time scale much shorter than the age of the Sun. Thus, these grains must be continually replenished, most likely through the break up of their parent bodies in the Kuiper Belt (Kenyon & Luu 1999). Energetic collisions can indeed lead to the disintegration of parent bodies and a catastrophic production of very small fragments (Fujiwara *et al.* 1977, Petit & Farinella 1993, Benz & Asphaug 1999). The KBO's can provide sufficiently frequent collisions to replenish the supply of small grains needed to account for the observed level of the zodiacal light provided 1) a non-negligible fraction of their total mass is contained in KBO's with  $< 1 - 100$  km, and 2) a modest fraction of these collisions actually lead to catastrophic fragmentation.

Asymmetric reradiation of stellar light by spinning bodies can lead to a torque on their orbits. This effect is commonly known as the Yarkovski (YORP) effect (Bottke *et al.* 2000, de Pater & Lissauer 2001). The characteristic YORP-induced orbital-evolution timescale for planetesimals with a density  $\rho_p$ , semi major axis  $a_i$ , and Keplerian speed  $v_K = (GM_*/a_i)^{1/2}$  is

$$\tau_Y \sim \pi c \rho_p s a_i^2 v_K / f L_* \tag{1}$$

where  $M_*$  and  $L_*$  are the mass and luminosity of the host star. The magnitude of the efficiency factor  $f$  is determined by the fractional amplitude of seasonal and diurnal temperature variations. The orbits of planetesimals with prograde spins expand as they experience a positive force (and  $f$ ) whereas planetesimals with retrograde spins undergo orbital decay with a negative  $f$ . The YORP effect enhances the PR drag for small particles. It can also lead to significant diffusion in the spacial distribution of km-size planetesimals during the main sequence life span of intermediate-mass stars. At 10 AU from stars with  $L_*$  ten times larger than that of the Sun, meter-size particles may undergo orbital decay within a Myr (see §3 below).

## 2.2. Debris disks around nearby intermediate-mass stars

In the quest to determine the properties and understand the origin of planets around other stars, it is often useful to identify their solar system analogs. Although it is impossible to directly detect residual planetesimals similar to the KBO's, the counterpart to the solar system zodiacal light have been found with Spitzer Space Telescope in the form of MIR and FIR excesses around

a significant fraction of nearby mature solar type stars (Rieke *et al.* 2004, Beichman *et al.* 2005, Moro-Martin *et al.* 2007, Hillenbrandt *et al.* 2008). Such excesses are assumed to be due to the reprocessed stellar radiation by debris dusty disks or rings at  $\sim 2 - 20$  AU from their host stars (Bryden *et al.* 2006, 2007, Trilling *et al.* 2008). The relevant-size grains are either blown away by radiation pressure or spiral toward their host stars due to radiation drag (both PR and YORP effects) on time scale much shorter than the age of the system (Artymowicz & Clampin 1997). They must be continually replenished by the collisions between relic planetesimals, analogous to the those in the Kuiper Belt and Oort Cloud (Kenyon & Bromly 2002, 2004, Wyatt *et al.* 2007, Moro-Martin *et al.* 2007, 2008).

The Spitzer Space Telescope’s detection threshold for these system is at levels at least an order of magnitude brighter than the outer solar Zodiacal light. It is entirely possible that all stars may have debris disks similar to that around the Sun. Some known debris disks have FIR excesses are  $10^{1-3}$  times larger than that associated with the zodiacal light in the solar system (Bryden *et al.* 2006). On average, the rate of collisional dust production is approximately proportional to the square of the surface density of their parent bodies. Presumably, stars with detected debris disks have richer reservoirs of relic planetesimals than the sun, albeit occasional major impacts may lead to brief episodic flare ups in the IR excess around individual systems (Kenyon & Bromly 2004, Grigorieva *et al.* 2007).

In the attempt to differentiate transient events and average properties, it may be fruitful to observationally determine the fraction of stars with detectable debris disks in a given population-analysis sample. In §1, we have already cited observational indications that  $\eta_d$  is an increasing function of  $M_*$ . This correlation of debris disks with the stellar mass can be partially attributed to observational selection effect because 1) A main sequence stars are generally younger and 2) their disks with similar fractional luminosity, relative to theirs, are brighter, warmer, and easier to detect than those around FGK dwarfs (Bryden, private communication). Nevertheless, this correlation is consistent with the expectation inferred from 1) the fraction of stars with planets, and 2) the disk accretion rate and mass around 1-3 Myr old stars are increasing functions of the stellar mass.

Further evidences for the collisional origin of debris-disk dust particles can be inferred from the general decline in the intensity of the debris disks with the age of individual host stars (Rieke *et al.* 2004). As a population, the fraction of A stars with  $70 \mu\text{m}$  excess decreases from 48 % around those younger than 30 Myr to 12 % for those older than 400 Myr. These signatures are consistent with the expectation that both dynamical and collisional processes lead to the depletion of these parent bodies. Nevertheless, a fraction of relatively massive A stars returns detectable debris disks throughout their main sequence lifespan.

The fraction planet-bearing FGK main sequence stars with FIR signature appears to be comparable to those without any known Jupiter-mass planets. After correcting some unfavorable ob-

servational selection effects, the intensity of the FIR excess for gas giant planet-bearing stars is  $\sim 3$  times that for stars without any planets, albeit the statistical significance of this correlation is weak (Bryden *et al.* 2007). In contrast to the strong correlation between the metallicity of FGK dwarfs and their planet-bearing probability (Fischer & Valenti 2005, Santos *et al.* 2005), there appears to be no correlation between it and detectable debris disks (Greaves *et al.* 2007). This dichotomy is probably due to the retention of debris-disk parent bodies depends much less sensitively on the surface density of planet-building blocks in their nascent disks (Wyatt *et al.* 2007) than the emergence of gas giant planets (Ida & Lin 2008a, b). However, the relatively high fraction of stars with planets around more massive (with mass  $M_* > 1 - 2M_\odot$ ) stars is independent of their metallicity (Pasquini *et al.* 2007). We have already indicated above that planet formation around the relatively massive stars may be more prolific not only because the protostellar disks around them have greater inventories of planet building blocks but also that the planetesimals formed more readily and are better retained in these disks.

Since both  $\eta_J$  and  $\eta_d$  increases with  $M_*$  and attain modest values (0.2 – 0.3) for intermediate-mass stars, a significant fraction of them (such as HR 8799 and Fomalhaut Kalas *et al.* 2008) may contain both. Our objective in this paper is to consider the dynamics of the planets and residual planetesimals during the post main sequence evolution of some intermediate-mass host stars.

### 3. A working model

Dynamical response of planets as a consequence of mass loss during the planetary nebula stage has been considered by several authors in the past mostly in the context of metal-rich DZ white dwarfs (Stern *et al.* 1990, Sackmann *et al.* 1993, Parriott & Alcock 1998, Siess & Livio 1999a, b, Debes & Sigurdsson 2002, Jura 2006).

For the origin of dusty disks in planetary nebulae, we consider similar effects, with a greater detailed treatment of both orbital dynamics and gas drag effects. We idealize the dynamics of the system into a series of interaction between three populations of objects: planetesimals with mass  $m_j$ , planets with mass  $M_j$ , and a central star with mass  $M_*$ .

There are two mean factors which influence the orbital change of a planet around the central star during the epoch of its mass loss: the change of the star’s mass, which reduces its gravity and causes the planet’s orbit to expand; and the gas drag by the outflow, which induces orbital decay. But the magnitude of this drag on a gas giant planet is negligible so that the equation of motion for the gas giant is reduced to the standard Kepler’s problem.

But the drag effect has a significant effect on the orbit of the planetesimal. In addition, it is also perturbed by the gravity of the planet. In a non rotating frame centered on the star, the equation



of motion of a planetesimal at a position  $\mathbf{r}_i$  can be expressed as

$$\frac{d^2\mathbf{r}_i}{dt^2} = -\frac{GM_*\mathbf{r}_i}{a_i^3} - \sum_j \frac{GM_j(\mathbf{r}_i - \mathbf{r}_j)}{|\mathbf{r}_i - \mathbf{r}_j|^3} - \sum_j \frac{GM_j\mathbf{r}_j}{r_j^3} - \frac{\mathbf{f}_i}{m_i} \quad (2)$$

where  $\mathbf{r}_j$  is the position of the planet and  $M_*$  is a function of time. On the right hand side of the above equation, gravity of the star and planet are expressed in the first two terms. The third term corresponds to the indirect force due to the rotation of the frame (Murray & Dermott 1999) and the fourth term represents the gas drag force on the particles.

In the Stoke's region, the magnitude of the drag force on a planetesimal by the wind of its host star can be expressed as

$$\mathbf{f}_i = \pi\rho_{wind}(s^2 + s_g^2)(\dot{\mathbf{r}}_i - \mathbf{v}_{wind})|\dot{\mathbf{r}}_i - \mathbf{v}_{wind}| \quad (3)$$

where  $v_{wind}$  is the wind velocity,  $s = (3m_i/4\pi\rho_p)^{1/3}$  and  $s_g = Gm_i/v_p^2$  are the physical and gravitational radius of a planetesimal with a mass  $m$  and density  $\rho_p$  (cf Supulver & Lin 2000). In the radial direction, this drag contribution is much smaller than the gravity from all three bodies. However, in the azimuthal direction, the drag slows down the planetesimals' initial Keplerian orbits (with a velocity  $v_K = (GM_*/r)^{1/2}$  at a distance of  $r$ ) to migrate inward on a characteristic time scale

$$\tau_{drag} = \left| \frac{r}{\dot{r}} \right| = \left| \frac{v_K}{2\dot{v}_K} \right| = \frac{v_K m_i}{2f_i} \simeq \frac{8\pi\rho_p s r^2 v_{wind}}{3\dot{M}_* v_K}. \quad (4)$$

In the above expression, we have neglected the gravitational focussing effect (which is small for km-size planetesimals) and assumed a steady spherically symmetric wind such that the background gas is determined by the stellar mass loss rate

$$\dot{M}_* = 4\pi r^2 \rho_{wind} v_{wind} \quad (5)$$

and the wind speed  $v_{wind}$  is generally assumed to be 10km/s which is larger than  $v_K$  for  $r$  greater than a few AU.

We can include other effects to the equations of motion. For example, the shape of some planetary nebulae significantly departs from spherical symmetry (O'Dell *et al.* 2004). In a follow up paper, we add a  $J_2$  component to the stellar gravity. It is also possible to include the gravity of additional stellar or planetary companions. In the current investigation, we neglect the PR and YORP effects during the AGB mass loss phase. Based on eq(1), we estimate that these effects can lead to significant orbital evolution during the brief AGB mass-loss phase (for  $\sim 10^4$  yr) only for sub-meter-size particles. Comparing eqs (1) and (4), we find that the hydrodynamic drag has a stronger impact on the orbital evolution of all particles at all locations if

$$\dot{M} > \dot{M}_Y \equiv 8fL_* v_{wind} / c v_K^2 \sim 10^{-6} M_\odot \text{yr}^{-1} \quad (6)$$

during the AGB mass loss phase.

However, during the main sequence life span  $\tau_*$  of A stars, YORP can induce residual planetesimals with sizes smaller than

$$s_Y = \tau_* f L_* / (\pi c \rho_p a_i^2 v_K) \sim (a_i / 10 \text{AU})^{3/2} \text{km} \quad (7)$$

to migrate over a significant fraction of their  $a_i$ . The inward migration of planetesimals may be halted after they are captured by the mean motion resonances of any embedded gas giants whereas the outward migration is limited to be less than  $10^2$  AU (see further discussions on the initial planetesimal reservoir below).

In order to fully explore possible range of initial conditions, we solve the equation of motion with a Hermit scheme which is kindly provided by Dr Sverre Aarseth (2003).

#### 4. Orbital evolution of planets and planetesimals due stellar mass loss

We recapitulate here the response of planets and planetesimals due to the changing gravitational potential during the rapid loss phase of their host AGB or post-AGB stars.

##### 4.1. Adiabatic orbital evolution of planets and large planetesimals

In our model, there are two main factors which affects the planet's orbital evolution: the reduction of the central mass and the gas resistance. The resistance term increases with  $s^2$  while the gravitational term increases with  $m_i \sim s^3$ . For relatively large planetesimals, gas resistance is unimportant and its orbital change is determined only by the central mass. Provided the time scale of the host star's mass loss  $\tau_M = |M_*/\dot{M}_*|$  is long compared with their Keplerian orbital time scale  $\tau_K = (a_i^3/GM_*)^{1/2}$ , the planetesimals' angular momentum  $h = vR$  does not change during this episode of mass loss, *i.e.* it is an adiabatic invariant. The planetesimal also retain their radial action so that a centrifugal balance is maintained in which  $v^2 = GM_*/a_i$ . Consequently,  $a_i = h^2/GM$  and the orbit expands as the host star loses mass (Duncan & Lissauer 1998).

In contrast, distant planets and planetesimals with  $\tau_K > \tau_M$  react to the impulsive change in the gravitational potential such that they would escape if their host stars lose more than half of their mass. During the AGB mass loss phase, the characteristic time scale for mass loss,  $\tau_M \sim 10^{4-5}$  yr. All planets and planetesimals with period less than  $\tau_M$  (or semi major axis within several 100 AU) undergo orbital expansion rather than escape.

The characteristic orbital expansion time scale is

$$\tau_{\text{exp}} = \left| \frac{a_i}{\dot{a}_i} \right| = \left| \frac{M_*}{\dot{M}_*} \right| = \tau_M. \quad (8)$$

From equations (4) and (8), we find that the magnitude of  $\tau_{\text{exp}} \simeq \tau_{\text{drag}}$  for particles with sizes

$$s \sim s_c \equiv \frac{3M_*}{8\pi\rho_p a_i^2} \left( \frac{v_K}{v_{\text{wind}}} \right) \simeq 0.1 \left( \frac{M_*}{M_\odot} \right)^{1.5} \left( \frac{1g \text{ cm}^{-3}}{\rho_p} \right) \left( \frac{a_i}{10\text{AU}} \right)^{-2.5} \left( \frac{10\text{km s}^{-1}}{v_{\text{wind}}} \right) \text{km}. \quad (9)$$

The above equation is applicable in the  $\rho_{\text{wind}} \propto 1/r^2$  (or  $v_{\text{wind}} = \text{constant}$ ) region of the stellar wind, and with the planet orbital radius greater than a few stellar radii. During the AGB mass loss phase, orbits of planetesimals with  $s > s_c$  expand during the stellar mass loss. Orbits of planetesimals with  $s \ll s_c$  undergo orbital decay on a time scale

$$\tau_{\text{drag}} \sim (s/s_c)\tau_M. \quad (10)$$

The relation of  $s_c$  with orbital radius is showed in Figure 1 which indicates a km-size planetesimal would be larger than  $s_c$  at  $r = 15$  AU from a mass-losing star so that its orbit would expands whereas it would be smaller than  $s_c$  at  $r = 10$  AU so that it would undergo orbital decay during the mass loss. This dependence arises because the gas density in a steady wind decreases with  $a_i$ . All planetesimals with sizes larger than  $s_c$  at their initial location are expected to expand, albeit with size-dependent speeds.

We are primarily interested in Kuiper-Belt equivalent regions because 1) that is the region where FIR from the debris disks implies the potential presence of a large population of residual planetesimals, 2) it is outside the region where gas giants are expected to form, and 3) it is also outside the quasi hydrostatic atmosphere of AGB's so that planetesimals may survive the evolution of their host stars prior to the AGB mass loss phase. For this region,  $s_c \sim 1$  km. In §2, we have already indicated that a significant fraction of the total mass in the Kuiper Belt may be contained in KBO's in this size range. In the above section, we also indicated that due to the YORP effect during the mean sequence evolution of their central stars, km-size KBO's (with  $s < s_Y$ ) have a tendency congregate near the outer mean motion resonances of long-period gas giants.

Around any given host star, the mass loss rate during the AGB mass loss phase may have large amplitude fluctuations. Since both the orbit expansion in response to the decreasing stellar mass and the gas drag in the stellar wind are proportional to the stellar mass loss rate,  $s_c$  is independent of  $\dot{M}$  [note that  $s_c$  is defined by  $\tau_{\text{exp}} \simeq \tau_{\text{drag}}$  and both  $\tau_{\text{exp}}$  and  $\tau_{\text{drag}}$  are inversely proportional to  $\dot{M}$ ]. Nevertheless, the magnitude of  $s_c$  decreases with the stellar mass. Also,  $\tau_K$  is large at relatively large  $a_i$  such that the condition for adiabatically may be violated during episodes of rapid mass loss when  $\tau_M$  is reduced below  $\tau_K$ . Nevertheless, planets and planetesimals can still be retained at large

distances provided the fractional loss of mass is limited during these brief events. Substantial mass reduction of the host stars can also cause dynamical instability of multiple-planet systems (Debes & Sigurdsson 2002). We will further explore this possibility in a subsequent paper.

#### 4.2. Entrainment of small planetesimals by the gas outflow

We demonstrate the orbital evolution of marginal and small planetesimals with numerical solutions of the equation of motion. In general, the orbits of intermediate ( $s \sim 1$  km) size, more distant ( $r \sim 10$  AU) planetesimals may enlarge at rates slower than the adiabatic expansion rates for the more massive and distant planetesimals.

If a planetesimal is comparable to or smaller than a critical size, orbital decay would be introduced due to gas drag. The gas drag would reduce the planetesimal’s momentum notably, and the angular momentum would not remain constant. From equations (2) and (3), we find that drag by the outwardly flowing gas exceeds the stellar gravity on particles smaller than

$$s_{\text{blowout}} \simeq \frac{r \rho_{\text{wind}} v_{\text{wind}}^2}{\rho_p v_K^2} \sim \frac{\dot{M}_* P_K v_{\text{wind}}}{\rho_p r^2 v_K} \quad (11)$$

where  $P_K$  is the orbital period. These very small particles ( $s < s_{\text{blowout}} \sim 1$  cm) are entrained by the stellar wind.

In order to quantitatively illustrate the divergent evolutionary paths of these particles, we consider a series of 4 planetesimals with radius of 10m, 100m, 1km and 10km all starting at 15Au from the star, whose orbits are initially without eccentricity. The mass of the star changes linearly from an initial value  $M_i = 3 M_\odot$  to a final value  $M_f = 0.5 M_\odot$  in 50,000 years. The orbital evolution of these planetesimals is shown in Figure 2. The 10 km object’s has a final orbital radius 6 time of the its initial value, which is exactly the reduction factor of the stellar mass. This correlation implies that the planetesimal’s orbital evolution is adiabatic. The  $s = 1$  km object also moves outward, but its expansion factor is considerably smaller than that of the 10 km-size planetesimal. The 100m object undergoes a small amount of orbital decay and its orbital evolution is stalled at 10 AU. The 10 m planetesimal quickly spiral into the central region and it is expected to be evaporated at about 10,000 years.

The processes of orbital decay (for planetesimals with  $s_{\text{blowout}} < s < s_c$ ) and entrained outflow (for planetesimals with  $s < s_{\text{blowout}}$ , due to the hydrodynamic drag by the outflowing gas, are equivalent to the Poynting-Robertson (PR) drag and radiative blow out by stellar radiation. During the AGB mass loss phases, hydrodynamic effects are much more intense than radiative effects.

### 4.3. Capture of small planetesimals by the planets' mean-motion resonances

In the above example, we neglected the presence of any major planets. Such planets also undergo adiabatic expansion during the planetary- nebula phase when their host stars lose a substantial fraction of their masses. For these large entities, the orbital expansion is adiabatic and take place on a time scale  $\tau_{\text{exp}} \simeq \tau_M$ . In addition, they exert dynamical perturbations on the nearby planetesimals, especially those on their low-order mean-motion resonances where their orbital periods are commensurate with each other in terms of small integers.

During the stellar mass loss, planets' orbits expand from their initial location  $r_p$  to their final location  $r_{\text{final}} = (M_i/M_f)r_p$ . Beyond these planets' orbits, small or marginal-size planetesimals, initially located at  $a_i$  (we will stick to  $r$  for the radius of planet, since it always keeps a circular orbit, and  $a$  for the semi-major axis for planetesimals.), either undergo orbital decay or expand at slower paces. Since their differential motion is determined by the gas drag effect, a planet and a (more distant) planetesimal cross each other's orbit on a time scale

$$\tau_{\Delta} \simeq \frac{(a_i - r_p)}{a_i} \tau_{\text{drag}}(s) = \frac{(a_i - r_p)}{a_i} \frac{s}{s_c} \tau_M. \quad (12)$$

Provided their initial location  $a_i < r_{\text{final}}$ , particles with sizes between

$$s_{\text{catchup}} \sim \frac{s_c a_i}{(a_i - r_p)} \quad (13)$$

and  $s_{\text{blowout}}$  generally undergo orbit crossing with the planet because the expansion of their orbits is slower than that of the planet.

Planetesimals along a planet's expansion path encounter its mean-motion resonances prior to their orbit crossing. Provided the duration  $\tau_{\Delta}$  across the width of these resonance ( $\Delta$ ) is long compared with the libration period near their centers ( $\tau_{\text{lib}}$ ) planetesimals would be captured onto the planets' mean-motion resonances (Murray & Dermott 1999). For example, a planet's 2:1 resonance has a finite effective width  $\Delta/r_p \simeq 2 \exp(1/2) (M_p/M_*)^{1/2}$ , where  $P_K = 2\pi\tau_K$  is the orbital period of the planet, and a libration period at its center  $\tau_{\text{lib}} \simeq (M_*/M_p)^{1/2} P_K / 2 \exp(1/2)$ . For this 2:1 resonance, the critical condition for capturing a planetesimal (with a size  $s$ ) is

$$M_p > \frac{s_c}{s} \frac{P_K}{4\tau_M \exp 1} M_*. \quad (14)$$

Planetesimals with  $s_{\text{catchup}} < s < s_{\text{rescap}}$  are captured onto the planet's 2:1 resonance where

$$s_{\text{rescap}} \simeq s_c \frac{P_k}{4\tau_M \exp 1} \frac{a_i}{1.6r_p} \frac{M_*}{M_p}. \quad (15)$$

In the above expression, the term  $a_i/1.6r_p$  is introduced to take into account of the stellar mass loss which is the cause of planet's orbital expansion. Equation (14) indicates that prior to reaching

$\sim 50 - 80$  AU, a Jupiter-mass planet would be able to capture exterior km-size planetesimals ( $s \simeq s_c (\sim 1 \text{ km})$ ) onto its 2:1 resonance. An Neptune-mass ice giant would also be able to capture these marginal-size planetesimals while its semi-major axis is  $< 10\text{AU}$ .

Planetesimals with initial semi-major axis  $a_i < 1.6r_p$  are already interior to the planet’s outer 2:1 resonance and they cannot be captured onto it. Also, relatively small ( $s < s_c$ ) planetesimals are unlikely to be captured onto the planet’s 2:1 mean motion resonances because their orbital decay is too rapid. However, this special location is the most distant lowest-order mean-motion resonance from the planet. There are many other lowest-order (such as 3:2 and 4:3) mean-motion resonances which are closer to the planet’s orbit. At these location, planet’s resonant capture probability is enhanced.

In the proximity of the planet, these lowest-order mean-motion resonances overlap with each other and planetesimals with negligible eccentricities and  $\Delta \simeq (12)^{1/2}R_R$  can enter into the planet’s Roche radius ( $R_R = (M_p/3M_*)^{1/3}r_p$ ) within a synodic period  $\tau_{\text{syn}} \simeq (3r_p/2\Delta)P_K$  (Lissauer 1987). Using a similar argument as above, the capture criterion becomes  $\tau_\Delta > \tau_{\text{syn}}$ , *i.e.* the planetesimals must not be able to diffuse through this “feeding zone” before they had an inferior conjunction. Thus, a fraction of planetesimals with

$$s < s_{\text{bypass}} = \frac{s_c}{18} \left( \frac{3M_*}{2M_p} \right)^{2/3} \frac{P_K \dot{M}_*}{M_*} \quad (16)$$

would be able to bypass the planet’s expanding orbit. For Jupiter-mass planets at  $\sim 30\text{AU}$  around typical intermediate-mass AGB stars,  $s_{\text{bypass}} \sim (1 - 10)s_c$ .

Although YORP effects can modify the radial distribution of km-size planetesimals during the host stars’ main-sequence phase (see §3), we neglect it in the determination of  $s_{\text{catchup}}$ ,  $s_{\text{rescap}}$ , and  $s_{\text{bypass}}$ . This approximation is adequate for the AGB mass loss phase provided the host stars’  $\dot{M} > \dot{M}_Y$  (see eq 6). During the mass-loss process, a planet’s orbit expands by a factor of  $M_i/M_f$ . Planetesimals with sizes in the range

$$s_{\text{bypass}} < s < s_{\text{catchup}} \quad (17)$$

are shepherded by the planet along its path. This size range is approximately an order of magnitude larger and smaller than  $s_c$ . A population of slightly larger ( $s_{\text{rescap}} < s < s_{\text{catchup}}$ ) and more distant (with initial  $a_i > 1.6r_p$ ) planetesimals are captured onto the planet’s 2:1 mean-motion resonances. Smaller or closer planetesimals may be also captured onto its other (such as 3:2 and 4:3) mean-motion resonances.

#### 4.4. Numerical calculation of resonant capture process

In order to illustrate the resonant capture process, we carried out a series of numerical calculations. In Figure 3, we plot the orbital evolution of a 0.1 km-size planetesimal. It has a density  $\rho_p = 3 \text{ g cm}^{-3}$  and it starts out with a circular orbit at 35 AU around a  $M_i = 4M_\odot$  star which linearly reduces its mass to  $M_f = 1M_\odot$  on a time scale of 100,000 yr through a wind with a speed  $v_{wind} = 10 \text{ km s}^{-1}$ . A planet with a mass  $M_p = 1 M_J$  was placed in a circular orbit at 20 AU initially. We also present the orbital evolution of the planetesimal when there is no giant planet in the system for comparison.

As mentioned before, the orbital radius of the giant planet only depends on the central stellar mass and initial orbit and adiabatically evolve from 20 AU to 80 AU. The planetesimal’s semi-major axis first decreases a little bit until about 30,000 years, when it is captured by the 3:2 mean-motion resonance with the giant planet. It’s also the time that the evolution tracks of the planetesimal with and without a giant planet in the system diverges. Before the capture point, the two tracks almost exactly overlap each other, while after that time, the resonance interaction pushes the planetesimal to move outward. Meanwhile, the ratio of the planetesimal’s semi-major axis to the planet’s becomes fixed on some value (in this case, the ratio is  $1.5^{\frac{2}{3}}$ ). Figure 4 shows the evolution of their period ratio. Starting from about 2.3 : 1 the ratio of the two periods decreases until the resonance point 3:2, and then it remains fixed on this value. During this process, although the period ratio passes 2:1 at about 10,000 years, the planetesimal was not captured by the planet’s 2:1 mean motion resonance.

As we have mentioned above that there are many factors which determine planetesimal’s resonant capture probability. First, for planetesimals with certain size, the initially positions of the planet and the planetesimals are important. Once the planet’s original orbit is set, only a range of initial position is appropriate for the planetesimals which would be captured. In Figure 5, we show the relation between initial positions and the final positions (semi-major axis) during the orbital evolution of several planetesimals with a range of sizes. In this model we adopt the same planetary system as in Figure 3: with a linear mass loss prescription for the host star (a constant loss rate from  $M_i = 4 M_\odot$  to  $M_f = 1 M_\odot$  within 100,000 yr and  $v_{wind} = 10 \text{ km s}^{-1}$ ). A  $1M_J$  planet is placed on an initial circular orbit with a radius 20 AU, and its orbit evolves to  $r_f = 80 \text{ AU}$ , according to the ratio of the star’s mass loss. All planetesimals have density  $\rho_p = 3 \text{ g cm}^{-3}$ . This figure shows that planetesimals with size in the range of 3km-30m could be captured onto the planet’s mean-motion resonance, including 2:1, 3:2 and 4:3 resonant point (period ratio). It shows that despite a wide range of initial positions, for planetesimals of the same size, only the ones with initial  $a_i$  in a ”critical range” could be captured onto the planet’s mean motion resonances. For example, among all the  $s = 300 \text{ m}$  planetesimals starting from 25 AU to 37 AU, only the ones with  $a_i$  between 27 AU and 31 AU could be captured onto 3:2 mean motion resonance.

Second, a planetesimal’s size is also a determining factor for resonant capture probability. Equation (15) indicates that the effective size range for resonant capture ( $s_{\text{rescap}} < s < s_{\text{scatchup}}$ ) depends on the planetesimal’s initial location  $a_i$ , so the ”critical range” of initial positions in the first point depends on the size of planetesimals. This dependence is confirmed by our numerical calculations. In Figure 5 the ”critical range” for  $s = 1$  km object to be captured onto 3:2 resonance is from 26 AU to 28 AU, while for  $s = 100$  m object is from 26 AU to 38 AU. The smaller planetesimals comparatively feel ”stronger” gas drag than larger ones at the same orbit, so they must have larger initial  $a_i$ ’s so that the gas drag is insufficient to drag them in and they have the possibility to being captured by the planet. Generally speaking, this ”critical range” is larger and further for small particles, as the picture demonstrates. These results are in good agreement with the above analytic estimates.

The magnitude of the gas drag is proportional to  $\rho_{\text{wind}}$  which is determined by the velocity of the gas wind and the mass loss rate of the central star. However, equation (9) indicate that  $s_c$  is essentially independent of  $\dot{M}_*$  and  $v_{\text{wind}}$ . Nevertheless  $s_{\text{rescap}}$  does depend on  $\tau_M$  and the star to planet’s mass ratio as well as planetesimals’ internal density (through  $s_c$ ). In order to explore these dependence, we consider variation in the model parameters from the standard model we have been working with above, *i.e.* with  $\dot{M} \sim 10^{-4} M_{\odot} \text{ yr}^{-1}$  and  $v_{\text{wind}} = 10 \text{ km s}^{-1}$ . These quantities may vary not only from star to star but also temporally around any host star. In addition, the initial and final mass of the stars determines the extent of planet’s orbital expansion and sweep up of the residual planetesimals. The internal density of the planetesimals ( $\rho_p$ ) may also have a range of possible values, from  $\sim 3 \text{ gm cm}^{-3}$  for asteroids to an order of magnitude smaller for comets.

Apart from the model parameters we have discussed above, we have adopted several different prescription for the evolution of the mass loss rate including constant, exponentially increasing, or ramp ups followed by declines. We find that once we have specified the initial and final stellar mass and the duration of the mass loss, our results are insensitive to variations in the mass loss rates. We also consider a range of planetary masses ( $1 - 10 M_j$ ) and eccentricities (0 and 0.1). Our results are also insensitive to the magnitude of these parameters.

In the present context, a planet’s final semi-major axis is generally less than 100 AU and its asymptotic period is  $< 1000$  yr. Thus, their orbital expansion is always adiabatic such that their orbits expand by a factor of  $M_i/M_f$ . By specifying the planet’s initial orbital radius, we can assess the inventory of planetesimals to be captured by the planet.

At which ratio of the orbital circle of the planetesimal and the planet would the particles be fixed is also determined by many factors. The rate of the orbital circle of the planetesimal and the planet would keep rising while no resonance happens. When it close to a resonance point, whether or not it could stop raising and stay is primarily determined by whether or not the resonance is strong enough, which is decided by factors like the gas’ density, the positions of the planetesimal



and the planet, etc. In our discussion, there are three major resonance points: rate of the orbital circle equals to 3:2, 4:3 and 3:2, while 3:2 is the most important one. It's shown in Figure 5. Take the curve of  $s = 300\text{m}$  planetesimals for example: the objects starting from  $a_i = 27\text{ AU}-31\text{ AU}$  are captured onto 3:2 resonance, with  $a_f$  around 105 AU; starting from  $a_i = 25\text{ AU}-26\text{ AU}$  are captured onto 4:3 resonance, which have  $a_f$  around 97 AU; and starting from  $a_i = 35\text{ AU}-36\text{ AU}$  are captured onto 2:1 resonance, which have  $a_f$  around 128 AU.

## 5. Collisional evolution of planetesimals and production of grains

In the previous section, we suggest that km-size icy particles are the preferred population of residual planetesimals for planets' resonance capture during the AGB mass loss phase of their host stars. In the next section, we first estimate the condition under which a population of such planetesimals may emerge at 10-100 AU prior to the AGB phase.

We then show that as a consequence of their orbital expansion and planets' sweeping process, these planetesimals' eccentricities increases to modest values and their collision frequency is strongly enhanced. We show that planetesimals orbit crossing with each other leads to frequent high-velocity disruptive impacts and the production of small grains. These grains can then reprocess the stellar radiation and produce the observed FIR rings around the white dwarf at the center of the helix nebula.

### 5.1. Inventory of planetesimals

In §2, we indicated that around typical progenitor of planetary nebula (A main sequence star), there may be a rich population of planetesimals. We now estimate their characteristic size prior to the mass loss from their host star.

There are two possible formation epochs for residual planetesimals (first few Myr and through out the main sequence life time of their host stars  $\tau_*$ ). First-generation planetesimals are formed in gas-rich protoplanetary disks. In such a gaseous environment, the velocity dispersion of the small planetesimals ( $\sigma$ ) is excited by their mutual interaction and damped by their interaction with the disk gas (Kokubo & Ida 2002). Due to hydrodynamic drag by the turbulent disk gas, these particles also undergo orbital decay (Supulver & Lin 2000). During this formative stage for their host star, largest planetesimals can grow to sizes well beyond a few km, especially in special locations such as the snow line and in the proximity of proto gas giants. They can also be scattered to large distances by the emerging planets (Zhou & Lin 2007). Nevertheless, we have already showed in the last section that during the planetary nebula stage, planetesimals with  $s > s_{\text{catchup}}$  retain their

semi-major axis ratio with respect to any embedded planet. They are unlikely to be captured onto any planet’s expanding mean-motion resonances.

Planetesimals can also grow *in situ* during the main sequence life span of their host stars ( $\tau_* \sim 10^{8-9}$  yr), long after the depletion of the disk gas. In this case, their  $\sigma$  is determined by their own collisional properties. Collisions can lead to both mergers and fragmentation. The condition for collisional fragmentation for basalt and ices have been extensively studied experimentally and simulated numerically (Stewart & Leinhardt 2008). In collisions between two comparable km-size aggregates, the critical impact speed  $v_{\text{frag}}$  for significant fragmentation is around a few meter per second (which is comparable to their surface escape speed  $v_g$  for these planetesimals). Shattering collisions are not only inhibits the coagulation of planetesimals but also introduces considerable energy dissipation. In Keplerian disks (such as Saturn’s rings), particles’ velocity dispersion ( $\sigma$ ) is determined by its excitation due to elastic scattering and damping due to inelastic collisions (Goldreich & Tremaine 1977, Bridges *et al* 1984). In gas-free disks with  $\sigma < v_{\text{frag}}$ , planetesimals undergo cohesive collisions with growing  $\sigma$  (Palmer *et al.* 1993, Aarseth *et al.* 1993). When their  $\sigma$  exceeds  $v_{\text{frag}}$ , collisions quench both mass and  $\sigma$  growth. In the absence of a dominant population of large planetesimals or embedded planets, planetesimals establish a collisional equilibrium in which their  $\sigma$  is approximately isotropic with  $\sigma \sim v_{\text{frag}}$ . An isotropic velocity dispersion implies that planetesimals can only collide with others in an annulus with a half width  $a_i\sigma/v_K$  and the magnitude of  $\sigma$  determines not only the collisional frequency but also the thickness of the planetesimal disk.

For km-size planetesimals,  $v_{\text{frag}} \sim v_g$  such that the collisional cross section of these planetesimals is mostly determined by their physical size. If most collisions are cohesive, the growth time scale ( $\tau_{\text{growth}}$ ) would be comparable to the collisional time scale ( $\tau_{\text{col}}$ )

$$\tau_{\text{growth}} \sim \tau_{\text{col}} \simeq (a_i/s)^2 (M_e/M_{\text{tot}}) (P_K/2\pi) \quad (18)$$

where  $M_e$  and  $M_{\text{tot}}$  are the individual and characteristic total (at  $a_i$ ) masses of planetesimals. The present estimates for  $M_{\text{tot}}$  in the Kuiper Belt ranges from a fraction to a few  $M_{\oplus}$  and that of debris disks around A stars may be near the upper end of this range (see §2). From equation (18), we find the characteristic size of planetesimals to be

$$s_{\text{char}} \simeq \left(\frac{30 \text{ AU}}{a_i}\right)^{1/2} \left(\frac{1 \text{ g cm}^{-3}}{\rho_p}\right) \left(\frac{\tau_{\text{growth}}}{\tau_*}\right) \left(\frac{\tau_*}{0.1 \text{ Gyr}}\right) \left(\frac{M_{\text{tot}}}{1 M_{\oplus}}\right) \text{ km}. \quad (19)$$

The above equation suggests that the spontaneous production of an isolated population of km-size planetesimals within the main sequence life span of a A star requires  $M_{\text{tot}}$  to be a few  $M_{\oplus}$ . This estimate is consistent with that simulated for the Kuiper Belt region (Kenyon & Bromley 2004).

In the derivation of  $s_{\text{char}}$ , we assume that  $\tau_{\text{growth}} \sim \tau_{\text{col}}$ , *i.e.* all collisions are cohesive. Since  $\sigma \sim v_{\text{frag}}$  some collisions are disruptive and  $s_{\text{char}}$  represents an upper limit in the planetesimals’

size distribution. In §2, we briefly show that the particle size distribution may follow a power law in which

$$dN/ds = (N_o/s_{\max})(s/s_{\max})^{-3.5} \quad (20)$$

where  $s_{\max}$  is the size of the largest particles and  $N_o$  is a normalization factor. With this size distribution, most of the mass are attained by the largest planetesimals. As long as  $s_{\text{char}} > 1$  km, there is always a supply of residual planetesimals which may be captured by the resonance of expanding planets.

Equation (19) implies a large potential dispersion in  $s_{\text{char}}$  around stars with different  $\tau_*$  and  $a_j$ . Perhaps the largest uncertainty is the total mass of residual heavy element  $M_{\text{tot}}$ . Around stars with relatively massive debris disks,  $s_{\text{char}} > 1$  km and the total mass of km-size planetesimals is

$$M_{\text{km}} \sim (1\text{km}/s_{\text{char}})^{1/2} M_{\text{tot}} \propto M_{\text{tot}}^{1/2}. \quad (21)$$

But, in less massive disks, the supply of km-size planetesimals may be limited. Based on this consideration and the uncertain fraction of A stars with planets, we do not expect the detection of trapped planetesimals around the remnant white dwarf at the center of every planetary nebula.

## 5.2. Eccentricity excitation

After km-size planetesimals are captured onto the planet’s mean-motion resonances, their orbital expansion would be locked provided the orbital migration time scale is longer than the resonant libration time scale *i.e.*  $\tau_M > \tau_{\text{lib}}$  or equivalently,

$$M_p > (M_*/4\text{exp}1)(P_K/\tau_M)^2 \sim 10^{-5} M_*. \quad (22)$$

Similar processes are found in the tidal evolution of Galilean satellites (Goldreich 1965, Lin & Papaloizou 1979, Peale & Yoder 1981) and migration of resonant planets (Lee & Peale 2002, Kley *et al.* 2004).

During their forced co-moving orbital expansion, the conservation of an adiabatic invariance induces the growth of resonant planetesimals’ eccentricity ( $e_s$ ) (Murray & Dermott 1999) on a time scale

$$\tau_{e,e} = e_s/\dot{e}_s = 2e_s^2\tau_{\text{exp}} = 2e_s^2\tau_M. \quad (23)$$

The above expression is for planetesimals in the planet’s 2:1 mean motion resonance. A similar expression can be derived for planet’s other mean-motion resonances.

Although the stellar outflow is in the radial direction, its drag on the planetesimals can also lead to the damping of their eccentricities on a time scale

$$\tau_{e,d} \simeq (s/s_c)\tau_M. \quad (24)$$

The above expression is derived from a linear perturbation analysis of equation (3) in the limit of small  $e_s$ . Comparison between  $\tau_{e,e}$  and  $\tau_{e,a}$ , it is apparent that planetesimals'  $e_s$  grows initially until an asymptotic equilibrium is established in which

$$e_e \sim (s/s_c)^{1/2}. \quad (25)$$

After they are captured by the planet at a location  $r_p = r_{\text{cap}}$ , the planetesimals' eccentricity growth may also be quenched by the termination of the stellar mass loss with an asymptotic

$$e_a \simeq (\ln(r_{\text{final}}/r_{\text{cap}}))^{1/2}. \quad (26)$$

In general, the eccentricity of co-moving resonant planetesimals is excited to the minimum of  $e_e$  and  $e_a$  which may both be a significant fraction of unity. (Both of these estimates on the asymptotic eccentricities break down as their values approach to unity.) Since the semi-major axes of the resonant planets are in lock-steps with that of the planet, the orbits of widely separated planetesimals overlap. The onset of orbit crossing creates opportunities for collisions between these planetesimals.

The eccentricities of distant planetesimals with period  $P_K \sim \tau_M$  (at  $a_i \geq 500$  AU) may also increase as a consequence of their marginally non-adiabatic adjustment to the host star's declining gravitational potential. However, these planetesimals' peri-center distances would not decrease significantly so that they are unlikely to venture into the regions of interest. At these large distances, planetesimals are sparsely populated, their collision frequency is also expected to be low.

In order to verify these analytic estimates, we show in Figure 6 the evolution of the planetesimal's eccentricity in the system in Figure 3. In this case, it remains negligible until 10,000 yr. when it encounters the planet's 2:1 mean-motion resonant point. Although not being captured, its eccentricity still slightly increases. When the planetesimal is captured onto the planet's 3:2 mean-motion resonance at 30,000 years, its eccentricity is evidently excited. At the end of our simulation it reaches its asymptotic value  $\sim 0.24$ . These result is in good agreement with the above discussions.

### 5.3. Collisional frequency and outcome

The results in Figure 6 can be generalized. In Figure 7, we show the asymptotic eccentricity distribution of a population of planetesimals (the system in Figure 3) verse their final orbital semi-major axis. It's very clear, as we pointed out before, there are three major resonance points of this system which can capture planetesimals onto co-moving orbits with giant planet and excite their eccentricities: 3:2 resonance point (the most important one, final semi-major axis of planetesimals

$a_f \sim 105$  AU); the 2:1 resonance point ( $a_f \sim 97$  AU) and 4:3 resonance point ( $a_f \sim 128$  AU). These three resonance points correspond to the three vertical bands on the plot. Once being excited, the eccentricity of the planetesimals will increase to about  $0.1 \sim 0.3$ . For planetesimals which are captured onto 3:2 resonant orbit, since their asymptotic semi-major axis is around 100 AU their orbits cross each other in the region between  $\sim 80 - 120$  AU. Thus the planetesimals' eccentricity excitation enlarges the radial extent of their impact zone from  $\sim a_i v_{\text{frag}}/v_K \sim 10^{-3} a_i$  to  $\sim 2e_s a_i \sim 0.4 a_i$ . This expansion greatly increases the pool of potential impactors.

As planetesimals along the expanding paths of the planet are captured onto its mean-motion resonances and co-moved by it to large distances, the surface number density  $\Sigma_p$  of planetesimals can increase by a factor  $f_\Sigma$  ( $\sim$  a few), depending on the initial distribution of  $\Sigma_p$  prior to the star's mass loss. (In this estimate, we took into account the growth of planetesimals' eccentricity associated with their resonantly forced orbital expansion.)

In contrast, the planetesimals' dispersion velocity in the direction normal to the disk plane does not change significantly (from its initial value  $\sigma \sim v_{\text{frag}}$ ) because the forcing by the mean-motion resonances is applied in the radial direction. (The velocity dispersion is no longer isotropic, *i.e.* the radial component of the velocity dispersion ellipsoid,  $\sigma_r \sim e_s v_K$ , becomes much larger than that in the direction normal to the orbital plane,  $\sigma_z \sim v_{\text{frag}}$ .) Consequently, the spacial density of resonant planetesimals ( $n'_p$ ) actually increases from their initial values ( $M_{\text{tot}}/(M_e 2\pi a_i^2 H)$  where  $H \sim \sigma_z a_i/v_K$  is the disk thickness) by a factor similar to  $f_\Sigma$  and the collisional frequency is enhanced by both the density and velocity enhancement. The characteristic collisional time scale  $\tau_{\text{col}}$  for the km-size planetesimals (which are trapped in the planet's mean-motion resonances) is reduced from its original magnitude to

$$\tau'_{\text{col}} \sim 1/(n'_p \sigma_r s^2) \sim \tau_{\text{col}} (v_{\text{frag}}/e_s v_K f_\Sigma) (1 \text{ km}/s_c)^{1/2} \sim (10^{-3} - 10^{-4}) (1 \text{ km}/s_c)^{1/2} \tau_*. \quad (27)$$

In the above expression, we assume that within the main sequence life span ( $\tau_*$ ) of the host star, *i.e.* prior to the AGB mass loss phase, perfectly cohesive collisions led to the formation of planetesimals with the power-law size distribution in equation (20) up to a size  $s_c$ .

During and after the AGB mass loss phase, the radial velocity dispersion associated with the asymptotic mean eccentricity ( $\sim 0.2$ ) is  $\sim 0.5 \text{ km s}^{-1}$  at  $\sim 100$  AU. Since this value of  $\sigma$  is much larger than  $v_{\text{frag}}$ , we anticipate all collisions during this stage will lead to powderization of the planetesimals. Since only km-size planetesimals are resonantly captured and co-move with the orbital expansion of the planet, production rate of fragment would be

$$\dot{M}_{\text{frag}} \sim (1 \text{ km}/s_c)^{1/2} M_{\text{tot}}/\tau'_{\text{col}} \sim (e_s v_K f_\Sigma/v_{\text{frag}}) (M_{\text{tot}}/\tau_*) \sim 10^{3-4} (M_{\text{tot}}/\tau_*). \quad (28)$$

With this erosion rate, the total mass of fragments produced during the AGB mass loss phase would be

$$M'_{\text{tot}} \sim \dot{M}_{\text{frag}} \tau_M \sim M_{\text{tot}} (10^{3-4} \tau_M/\tau_*). \quad (29)$$

During the mass loss epoch, the magnitude of  $\tau'_{\text{col}}$  can be reduced to  $\sim 10^{4-5}$  yr which would be comparable to  $\tau_M$ . In these systems, a significant fraction of  $M_{\text{tot}}$  could be fragmented through these disruptive processes. Since the emergence of km-size planetesimals requires  $M_{\text{tot}}$  to be a few  $M_{\oplus}$ , we anticipate that in planetary nebula where they coexist with some gas giants, the total mass of their fragmentary debris ( $M'_{\text{tot}}$ ) may indeed exceed that of the Earth.

Fragments' mass spectrum, immediately after the disruptive impacts, depends on the highly uncertain material strength of planetesimals. If these planetesimals are loosely bound aggregates high speed ( $\sim \text{km s}^{-1}$ ) impacts may disperse them down to the sizes of their basic building blocks. For simplicity, we assume a power-law size distribution as expressed in equation (20). In this case, a major portion of  $M'_{\text{tot}}$  is contained in the largest fragments (with  $s = s_{\text{max}}$  and mass  $m_{\text{max}} = 4\pi\rho_p s_{\text{max}}^3/3$ ) so that the normalization factor can be derived from equation (20) to be  $N_o = M'_{\text{tot}}/2m_{\text{max}}$ . In the absence of reliable experimental data, we infer below the magnitude of  $s_{\text{max}}$  using the flux of reprocessed radiation from the ring around WD 2226-210.

#### 5.4. Reprocessed radiation by the residual fragments

Another implication of the power-law size distribution is the fraction of stellar photons which may be absorbed and scattered by the fragments. In the calculation on the intensity of reprocessed radiation at any instance of time, we need to take into consideration the potential depletion of all particles. We have already indicated above that, during the gas loss phase, fragments with sizes  $s < s_{\text{blowout}}$  are continually entrained and removed by the outflowing gas from the location of their production on a time scale  $\tau_{\text{fly}} \sim a_i/v_{\text{wind}}$ . Similarly, inward orbital decay of fragments in the size range  $s_{\text{blowout}} < s < s_{\text{bypass}}$  proceeds on a time scale  $\tau_{\text{drag}} = (s/s_c)\tau_M$  (equation (10)) are not inhibited by the planet's tidal barrier during their orbital decay.

In the calculation of intensity of reprocessed stellar irradiation at a particular wavelength range ( $\lambda$ ), we also need to include a reduction factor ( $s/\lambda$ ) for emissivity of small particles (in the range from  $s_{\lambda} \equiv \lambda > s$  down to a minimum grain size  $s_{\text{min}}$ ). In the limit  $s_{\text{bypass}} \sim s_c > s_{\text{blowout}} > s_{\lambda} > s_{\text{min}}$ , the total area covered by the fragments in the impact zone would be

$$\sigma_{\text{zone}} = \left( \int_{s_{\text{bypass}}}^{s_{\text{max}}} + \int_{s_{\text{blowout}}}^{s_{\text{bypass}}} \frac{\tau_{\text{drag}}}{\tau_M} + \int_{s_{\lambda}}^{s_{\text{blowout}}} \frac{\tau_{\text{blowout}}}{\tau_M} + \int_{s_{\text{min}}}^{s_{\lambda}} \frac{s}{\lambda} \right) \pi s^2 \frac{dN}{ds} ds. \quad (30)$$

Neglecting the YORP effect and inserting expressions for  $dN/ds$  in equation (20), we find that

$$\begin{aligned} \sigma_{\text{zone}} \sim & 2\pi N_o s_{\text{max}}^2 \left\{ \left[ \left( \frac{s_{\text{max}}}{s_{\text{bypass}}} \right)^{1/2} - 1 \right] + \frac{s_{\text{max}}}{s_c} \left[ \left( \frac{s_{\text{bypass}}}{s_{\text{max}}} \right)^{1/2} - \left( \frac{s_{\text{blowout}}}{s_{\text{max}}} \right)^{1/2} \right] \right. \\ & \left. + \frac{\tau_{\text{fly}}}{\tau_M} \left[ 2 \left( \frac{s_{\text{max}}}{s_{\lambda}} \right)^{1/2} - \left( \frac{s_{\text{max}}}{s_{\text{blowout}}} \right)^{1/2} - \left( \frac{s_{\text{max}}}{s_{\lambda}} \right) \left( \frac{s_{\text{min}}}{s_{\text{max}}} \right)^{1/2} \right] \right\}. \quad (31) \end{aligned}$$

Although AGB stars'  $L_*$  can reach  $\sim 10^{-3}L_\odot$  to exert non-negligible YORP effect on km-size planetesimals at  $\sim 10 - 100$  AU, this phase is brief and does not significantly affect their orbits.

In the limit  $s_c \sim s_{\text{bypass}}$ ,  $\sigma_{\text{zone}} \sim 4\pi N_o s_{\text{max}}^{5/2} s_{\text{bypass}}^{-1/2}$ . Interior to the impact zone and the planet's orbit, fragments with  $s_{\text{bypass}} > s_{\text{blowout}} > s_\lambda$  contributes to  $\sigma_{\text{interior}} \sim (2\pi N'_o s_{\text{max}}^3 / s_c) [(s_{\text{bypass}} / s_{\text{max}})^{1/2} - (s_{\text{blowout}} / s_{\text{max}})^{1/2}] \sim 2\pi N'_o s_{\text{max}}^{5/2} s_{\text{bypass}}^{-1/2} < \sigma_{\text{zone}}$  because the normalization factor  $N'_o$  (which is determined by the resonant capture efficiency) is expected to be smaller than  $N_o$ . Exterior to the impact zone, small fragments ( $s < s_{\text{blowout}}$ ) contributes to  $\sigma_{\text{exterior}} \sim (2\pi N_o s_{\text{max}}^2 \tau_{\text{fly}} / \tau_M) [2(s_{\text{max}} / s_\lambda)^{1/2} - (s_{\text{max}} / s_{\text{blowout}})^{1/2} - (s_{\text{max}} / s_\lambda)(s_{\text{min}} / s_{\text{max}})^{1/2}] \sim \sigma_{\text{zone}} (s_{\text{bypass}} / s_\lambda) (\tau_{\text{fly}} / \tau_M)$  which may also be much smaller than  $\sigma_{\text{zone}}$ .

Equations (11) and (16) indicate that both  $s_{\text{blowout}}$  and  $s_{\text{bypass}}$  increases with  $\dot{M}_*$ . After the host star attains its  $M_f$  (as in the case of the white dwarf WD 2226-210 at the center of the Helix nebula), the mass flux of gas outflow is significantly reduced. While the eccentric resonant-captured planetesimals continue to collide with each other on a time scale  $\tau'_{\text{col}}$  and generate fragments at a rate  $\dot{M}_{\text{frag}}$ . When both  $s_{\text{blowout}}$  and  $s_{\text{bypass}}$  decreases below  $s_\lambda$ , equation (31) is much simplified by a continuous power-law size distribution (as in equation 20) to

$$\sigma_{\text{zone}} \sim 2\pi N_o s_{\text{max}}^2 \left[ \left( \frac{s_{\text{max}}}{s_\lambda} \right)^{1/2} - 1 \right]. \quad (32)$$

In this case, the fragments are confined to the impact zone.

Finally, the particle size distribution may also be truncated at the lower ranges the radiative blow out process ( $s_\gamma$ ). In that limit,  $s_\lambda$  would be replaced by  $s_\gamma$  in the above expressions.

## 6. Structure of the disk around WD2226-210

The proximity of WD2226-210 at the center of the Helix nebula has been imaged in multiple wavelength. The observed spectral energy distribution (SED) has been analyzed in terms of a disk of dust grains which are assumed to have the same astronomical size distribution as equation (20) and a size range between 60-1000  $\mu\text{m}$  (Su *et al.* 2007). (The lower size limit is set ( $s_{\text{min}} = 60\mu\text{m}$ ) by the condition for radiative blow out (*i.e.*  $s_\gamma$ ), albeit  $s_{\text{max}}$  is arbitrarily set.) The total area covered by these dust grains is inferred to be  $\sigma_{\text{tot}} \sim 6 \times 10^{27} \text{ cm}^2$  distributed over a distance between 35-150 AU. For the assumed range of grain sizes, their total mass is inferred to be  $M_{\text{grain}} \sim 0.1 M_\oplus$ . (This mass is inferred from the assumed size distribution in equation 20, neglecting the contribution of hydrodynamic blow out and drag on the small grains in equation 31). The magnitude of

$$M_{\text{grain}} \sim 0.1 (s_{\text{max}} / 0.1 \text{ cm})^{1/2} M_\oplus \quad (33)$$

if the assumed size distribution extends to grains larger than  $1000 \mu\text{m}=0.1 \text{ cm.}$ ) Since the present and past PR drag time scale for these grains ( $\sim 10 \text{ My}$ ) is  $< \tau_*$ , they must be continually replenished, presumably through the powderization of their parent-body residual planetesimals. Su *et al.* (2007) estimated the current collision time scale for  $100\mu\text{m}$  grains to be  $\sim 0.1 - 1 \text{ My}$  which is  $> \tau_M$ .

Although this model provides a reasonable fit to the observed SED, a challenging theoretical issue is whether the grains' parent bodies may have sufficient collision frequencies to generate so many fragments despite their (parent bodies') much smaller surface area to volume ratio. If the generation of  $M_{\text{grain}}$  requires a substantially more massive ( $\gg M_{\oplus}$ ) population of parent bodies, its protracted retention during the main sequence life span of their host stars would need to be addressed rather than assumed.

We now apply the results in the previous sections to provide some quantitative justification for the model proposed by Su *et al.* (2007). In §2, we cite evidences that both gas giant planets and debris disks are commonly found around A stars. In our model, we consider the possibility that the progenitor star of WD 2226-210 was surrounded by one or more gas giant planets (at distances comparable to those around Uranus and Neptune) and a debris disk similar to the Kuiper Belt in the solar system. In previous chapters, we have already showed that in debris disks which contain a few (or more)  $M_{\oplus}$  within  $\sim 100 \text{ AU}$ , a population of km-size planetesimals (with a total mass  $M_{\text{rmtot}} > 1 M_{\oplus}$ ) can form through inelastic and cohesive collisions (with a velocity dispersion  $\sigma \sim v_{\text{frag}} \sim \text{a few m s}^{-1}$ ) during the main sequence life span of type A stars (*i.e.* within  $\tau_* \sim 100 \text{ My}$ ). Due to the combined planetary tidal perturbation and the YORP effect, a fraction of these residual planetesimals may accumulate near the planets' outer mean motion resonances.

During the AGB mass loss phase when most of the stellar mass is rapidly lost, semi-major axes of both planets and relatively large residual planetesimals increases as  $M_*^{-1}$ . In contrast, the outflowing wind imposes hydrodynamic drag on the planetesimals and causes those with relatively small sizes ( $s < s_c \sim 1\text{km}$ ) to undergo orbital decay. When they cross the planet's expanding path, these small planetesimals are captured onto its mean motion resonances of the planets.

During the subsequent shepherd orbital expansion, the resonant planetesimals are swept up with enhance surface densities (by a factor  $f_{\Sigma} \sim \text{a few}$ ), excited eccentricities ( $e_s \sim e_e$  or  $e_d$  which can be up to a significant fraction of unity), and highly anisotropic velocity dispersion ( $\sigma_r \sim e_s v_K \sim 10^{2-3} \sigma_z$ ). The collisional time scale for these planetesimals are greatly reduced (by a factor  $\sim 10^{3-4}$ ) from  $\tau_*$  to  $\sim \tau_M$  so that a significant fraction of the planetesimals captured on the planet's mean-motion resonances may actually collide with each other. The impact speed of these collisions ( $\sim \sigma_r \sim 0.5\text{km s}^{-1}$ ) is sufficiently large to pulverize km-size planetesimals to very small pieces.



The actual size of the largest fragments ( $s_{\max}$ ) is poorly determined. However, we can infer it by assuming  $M_{\text{grain}} \simeq M'_{\text{tot}}$  (from equations 33 and 29) and  $\sigma_{\text{tot}} \sim \sigma_{\text{zone}}$  (from equations 31 or 32). If we neglect any residual stellar winds and self-consistently adopt  $M'_{\text{tot}} \sim M_{\text{tot}} = 1 M_{\oplus}$ , we would infer  $s_{\max} \sim 10\text{cm}$ .

In the absence of significant stellar wind, hydrodynamic blowout and drag are negligible. Whereas radiation blow out remove smallest grains (with  $s < 60\mu\text{m}$ ), the PR drag causes intermediate-size ( $\sim 100\mu\text{m}$ ) grains to undergo orbit decay on a time scale ( $\tau_{\text{PR}}$ ) of 3-50 Myr over this region (between 35-150AU). Since this time scale is much longer than the time lapse since the AGB mass loss phase around WD 2226-210, it has negligible effect on the ring at the center of the Helix nebula. But around mature white dwarfs (with  $\tau_* > \tau_{\text{PR}}$ ), it is possible for

$$\tau_{\Delta}(\Delta = R_R, \tau_{\text{decay}} = \tau_{\text{PR}}) > \tau_{\text{syn}} \quad (34)$$

or equivalently,  $\tau_{\text{PR}} > (M_*/M_p)^{2/3} P_K$ . In this limit, these grains may not be able to bypass the planet's orbit so that their asymptotic surface density distribution (around older white dwarfs) may bear the signature of planet's tidal barrier and have an inner edge (Wyatt *et al.* 1999). Nevertheless, one or more eccentric planets can disable the orbits of these planetesimals, especially after a substantial loss of  $M_*$  (Levison *et al.* 1994) This process may also provide a supply of heavy elements to pollute the atmosphere of DZ white dwarfs (Debes & Sigurdsson 2002). We will consider that effect elsewhere.

In the case of WD 2226-210 at the center of the Helix nebula, there may still be a reduced but non negligible stellar wind. Due to hydrodynamic drag (rather than stellar photons), sub-mm grains are may be blow away while slightly larger grains may undergo orbital decay and bypass any embedded planets. In this limit, grain depletion would lead to transitions in their size distribution. The inferred values of  $s_{\max}$  could be reduced by the depletion of the small particles.

Finally, we consider possible observable consequence of this process. During the planetary nebula, embedded planets may also accreted gas from the outflowing stellar wind at a rate

$$\dot{M}_g \simeq \left(\frac{M_p}{M_*}\right)^2 \left(\frac{v_K}{v_{\text{wind}}}\right)^4 \dot{M}_*. \quad (35)$$

The above equation is derived from a modified Bondi accretion formula. For a Jupiter mass planet, the total accreted gas during the AGB mass loss phase ( $\sim \dot{M}_g \tau_M$ ) would be a small fraction ( $\sim M_p/M_*$ ) of its own mass. Nevertheless, it could provide an accretion luminosity (up to  $\sim 10^{-4}L_{\odot}$ ) which may be marginally detectable by ALMA against the ring background.

The hot white dwarf WD 2226-210 at the center of the Helix nebula provides an intense source of UV radiation. The ionization of planetary atmosphere can lead to its photoevaporation and mass loss (Lammer *et al.* 2003, Baraffe 2004, 2005, Murray-Clay *et al.* 2009). Lyman

$\alpha$  absorbing clouds have been observed around a close-in planet, HD 209458b (Vidal-Madjar *et al.* 2003). Its extension beyond the planet’s roche lobe has been attributed to be a signature of outflow, albeit the inferred mass loss rate remains uncertain (Ben-Jaffel 2007). The energy flux of ionizing photons irradiated onto the surface of gas giants located at  $\sim 30$  AU from WD 2226-210 is 2-3 orders of magnitude larger than that onto hot Jupiters around solar type stars. Scaling from the radiative hydrodynamic models for HD 209458b (Murray-Clay *et al.* 2009), we do not expect long-period gas giants to lose significant fraction of their mass during the AGB mass loss phase. Nevertheless, photoionizing stellar photons may induce emission of signature spectral lines on the extended planetary envelope which may potentially be detectable with high dispersion spectroscopic observations (we thank Y.-H. Chu for this suggestion).

Mean motion resonant capture of km-size planetesimals by one or more embedded planets and their subsequent lock-step orbital migration also lead to their non axisymmetric surface density distribution (Murray-Clay & Chiang 2005). In principle, such a structure can be resolved with sub arc second imaging. However, the observed IR radiation is due to reprocessed stellar radiation by the fragments of high-speed collisions. Their recoil velocity may be sufficient to smear out such a structure. However, multi-wavelength resolved images may reveal a particle size dependence in the grains radial distribution. The detection of very small ( $s < s_{\text{blowout}}$ ) grains at large disk radii and intermediate  $s$  ( $s_{\text{blowout}} < s < s_{\text{bypass}}$ ) would provide supporting evidence for our scenario.

## 7. Summary and discussion

In this paper we construct a dynamic model for the post main sequence evolution of planetary systems. With this model, we find that as a consequence of mass loss from the central star, km-size planetesimals can be captured by mean-motion resonance and form a disk beyond the planets. During the subsequent orbital expansion, the eccentricity of the resonant planetesimals is excited which enhances their collision frequency. Highly destructive impacts among these planetesimals can continuously provide a ring of dust around the mature star, which can be seen in the FIR and MIR wave band. This phenomenon can also be extended to other A-F stars, with the inference that a large fraction of stars may have planet systems and substantial debris disks during their main sequence epoch. Stars with higher main sequence mass, greater mass loss rate and lower velocity of star wind tend to have higher ability to capture the planetesimals.

We applied this model to account for the dust ring around WD 2226-210 at the center of the Helix nebula. It can also be used to study other young white dwarfs. For example, we anticipate this process will occur when the Sun evolve to its AGB mass loss phase, albeit among of fragmentary dust would be limited and the intensity of the reprocessed radiation may be weak. Since this process depends sensitively on the initial heavy element content and the presence of sufficiently

massive planets, we expect there to be large dispersion in the signatures of dust debris around young white dwarfs. Nevertheless, we expect to see more dusty rings around planetary nebulae with A star progenitors because the fractions of stars with planets and debris disks is observed to increase with stellar mass.

The present work is developed for the  $\rho_{wind} \propto 1/r^2$  (or  $v_{wind} = \text{constant}$ ) portion of a stellar wind and thus not applicable to the region very close to the star. In addition, apart from the planetesimals that are captured by the planet, the fate of other planetesimals also need to be discussed. These may also play an important role in the evolution of the white dwarf.

Some observational tests of these models should be possible with present technology or will be possible soon. As the planetesimals are collected by the giant planet, it is most likely that the gas giant planet survives the AGB period, and the orbit changes to several times the original one. If such giant planet around white dwarf can be detected, it would provide support to our model. Although there are several failed attempts in these searches (Debes *et al.* 2005a, b, 2007), the upper mass limits set for the unseen planet is far larger than that needed in our model.

We thank Sverre Aarseth for provide the Hermit integrator, Y.-H. Chu and an anonymous referee for useful correspondence and helpful suggestions. This work is supported by NSFC(10233020), NCET (04-0468), NASA (NNX07A-L13G, NNX07AI88G, NNX08AM84G), JPL (1270927), and NSF(AST-0908807).

## REFERENCES

- Aarseth, S. J., Lin, D. N. C. & Palmer, P. L. 1993 ApJ, 403, 351
- Artymowicz, P. & Clampin, M. 1997, ApJ, 490, 863
- Backman, D. E., Dasgupta, A. & Stencel, R. E. 2005, ApJ, 450, L35
- Baraffe, I., Chabrier, G., Barman, T.S., Selsis, F., Allard, F., & Hauschildt, P.H. 2005, A.&A., 436, L47
- Baraffe, I., Selsis, F., Chabrier, G., Barman, T.S., Allard, F., Hauschildt, P.H. & Lammer, H. 2004, A.&A., 419, L13
- Beichman, C. A., Bryden, G., Rieke, G. H., Stansberry, J. A., Trilling, D. E., Stapelfeldt, K. R., Werner, M. W., Engelbracht, C. W., Blaylock, M., Gordon, K. D., Chen, C. H., Su, K. Y. L. & Hines, D. C. 2005, ApJ, 622, 1160

- Beichman, C. A., Bryden, G., Stapelfeldt, K. R., Gautier, T. N., Grogan, K., Shao, M., Velusamy, T., Lawler, S. M., Blaylock, M., Rieke, G. H., Lunine, J. I., Fischer, D. A., Marcy, G. W., Greaves, J. S., Wyatt, M. C., Holland, W. S. & Dent, W. R. F. 2006, ApJ, 652, 1674
- Ben-Jaffel, L., 2007, ApJ, 671, L61.
- Benz, W. & Asphaug, E. 1999, Icar, 142, 5
- Bernstein, G. M., Trilling, D. E., Allen, R. L., Brown, M. E., Holman, M. & Malhotra, R. 2004, AJ, 128, 1364
- Blocker, T. 1995, A.Ap, 299, 755
- Bottke, W.F.Jr., Rubincam, D.P., & Burns, J.A. 2000, Icarus, 145, 301
- Bridges, F., Hatzes, A.P., & Lin, D.N.C., 1984, Nature, 309, 333
- Brown, P. J. *et al.* 2005, ApJ, 635, 1192
- Bryden, G., Beichman, C. A., Trilling, D. E., Rieke, G. H., Holmes, E. K., Lawler, S. M., Stapelfeldt, K. R., Werner, M. W., Gautier, T. N., Blaylock, M., Gordon, K. D., Stansberry, J. A. & Su, K. Y. L. 2006, ApJ, 636, 1098
- Clarke, C. J., Pringle, J. E. 2006, MNRAS, 370L, 10
- Cumming, A., Butler, R. P., Marcy, G. W., Vogt, S. S., Wright, J. T. & Fischer, D. A. 2008, PASP, 120, 531C
- Cuzzi, J. N., Pollack, J. B. & Summers, A. L. 1980, Icar, 44, 683
- Debes, J. H. & Sigurdsson, S. 2002 ApJ, 572, 556
- Debes, J. H., Sigurdsson, S. & Woodgate, B. E. 2005, ApJ, 633, 1168
- Debes, J. H., Sigurdsson, S. & Woodgate, B. E. 2005, AJ, 130, 1221
- Debes, J. H., Sigurdsson, S. & Hansen, B. 2007, AJ, 134, 1662
- De Pater, I. & Lissauer, J.J. 2001, Planetary Science
- Dollinger, M.P., Hatzes, A.P., Pasquini, L., Guenther, E.W., Hartmann, M., Girardi, L., & Esposito, M. 2007. A & A, 472, 649
- Duncan, M. J. & Quinn, T. 1993, ARA & A, 31, 265

- Duncan, M., Quinn, T. & Tremaine, S. 1987, AJ, 94, 1330
- Farinella, P. & Davis, D. R. 1996, Sci, 273, 938
- Fischer, D. A. & Valenti, J. 2005, ApJ, 622, 1102
- Fujiwara, A., Kamimoto, G. & Tsukamoto, A. 1977, Icar, 31, 277
- Garcia L., R., Natta, A., Testi, L., Habart, E. 2006, A & A, 459, 837
- Gautier, T. N., III, Rieke, G. H., Stansberry, J., Bryden, G. C., Stapelfeldt, K. R., Werner, M. W., Beichman, C. A., Chen, C., Su, K., Trilling, D., Patten, B. M. & Roellig, T. L. 2007, ApJ, 667, 527
- Goldreich, P. 1965, Natur, 208, 375
- Gould, A. *et al.* 2006, ApJ, 644L, 37
- Gradie, J. C., Chapman, C. R. & Tedesco, E. F. 1989, *aste, conf*, 316
- Greaves, J. S., Fischer, D. A., Wyatt, M. C., Beichman, C. A. & Bryden, G. 2007, MNRAS, 378L, 1
- Griffin, R. E. M.; David, M. & Verschueren, W. 2000, A & AS, 147, 299
- Grigorieva, A., Artymowicz, P. & Thèbault, Ph. 2007, A & A, 461, 537
- Hartmann, W.K. 1999, M & PS, 34, 167
- Hatzes, A.P. 2008, Phys Scr, T130, 014004
- Ida, S. & Lin, D. N. C. 2004, ApJ, 604, 388
- Ida, S. & Lin, D. N. C. 2004, ApJ, 616, 567
- Ida, S. & Lin, D. N. C. 2005, ApJ, 626, 1045
- Ida, S. & Lin, D. N. C. 2008, ApJ, 616, 567
- Ida, S. & Lin, D. N. C. 2008, ApJ, 685, 584
- Jewitt, D. C. & Luu, J. X. 1997, 1995, AJ, 109, 1867
- Johnson, J. A., Butler, R. P., Marcy, G. W., Fischer, D. A., Vogt, S. S., Wright, J. T., Peek, K. M. G. 2007 ApJ, 670, 833

- Jura, M. 2006 ApJ, 653, 613
- Kennedy, G. M., Kenyon, S. J., & Bromley, B. C. 2007, Ap & SS, 311, 9
- Kenyon, S. C. & Bromley, B. C. 2002, ApJ, 577L, 35
- Kenyon, S. C. & Bromley, B. C. 2004, AJ, 127, 513
- Kenyon, S. C. & Luu, J. X 1999, AJ, 118, 1101
- Kley, W., Peitz, J. & Bryden, G., 2004, A.&A., 414, 735
- Kokubo, E. & Ida, S. 2002, ApJ, 581, 666
- Kretke, K. A. & Lin, D. N. C., 2007 ApJ, 664L, 55
- Kretke, K. A., Lin, D. N. C. & Turner, N. J. 2009, ApJ, 690, 407
- Kwok, S. 1982, ApJ, 258, 280
- Laughlin, G., Steinacker A. & Adams, R., 2004, ApJ, 608, 489
- Laor, A. & Draine, B. 1993 ApJ, 402, 441
- Lee, M. H. & Peale, S. J. 2002, ApJ, 567, 596
- Levison, H. F., Duncan, M. J. & Wetherill, G. W. 1994, Natur, 372, 441
- Lin, D. N. C. & Papaloizou, J. 1979, MNRAS, 188, 191
- Lissauer, J.J. 1987, Icarus, 69, 249
- Mathis, J. S., Rumpl, W. & Nordsieck, K. H 1977, ApJ, 217, 425
- Marois, C., Macintosh, B., Barman, T., Zuckerman, B., Song, I., Patience, J., Lafrenière, D. & Doyon, R. 2008, Sci, 322, 1348
- Moro-Martin, A., Wyatt, M. C., Malhotra, R. & Trilling, D. E. 2007, astro.ph, 3383
- Moro-Martin, A., Malhotra, R., Carpenter, J. M., Hillenbrand, L. A., Wolf, S., Meyer, M. R., Hollenback, D., Najita, J. & Henning, T. 2008, ASPC, 398, 333
- Murray, C. D. & Dermott, S. F. 1999, Solar system dynamics, Princeton university press
- Murray-Clay, R.A. & Chiang, E.I. 2005, ApJ, 619, 623
- Murray-Clay, R.A., Chiang, E.I. & Murray, N. 2009, ApJ, 693, 23

- Natta, A., Testi, L., Randich, S. 2006, *A & A*, 452, 245
- O'Dell, C. R., McCullough, P. R. & Meixner, M. 2004, *AJ*, 128, 2339
- Palmer, P. L., Lin, D. N. C. & Aarseth, S. J. 1993, *ApJ*, 403, 336
- Parriott, J. & Alcock, C. 1998 *ApJ*, 501, 357
- Pasquini, L., Dollinger, M.P., Weiss, A., Girardi, L., Chevaro, C., Hatzes, A.P., da Silva, L. & Satiawen, J. 2007, *A & A*, 473, 979
- Yoder, C. F. & Peale, S. J. 1981, *Icar*, 47, 1
- Petit, J.-M. & Farinella, P. 1993, *CeMDA*, 57, 1
- Rieke, G. H., Su, K. Y. S., Stansberry, J. A., Trilling, D., Bryden, G., Muzerolle, J., Young, E. T., Beichman, C. A. & Stapelfeldt, K. R. 2004, *AAS*, 205, 1120
- Rieke, G. H., Su, K. Y. L., Stansberry, J. A., Trilling, D., Bryden, G., Muzerolle, J., White, B., Gorlova, N., Young, E. T., Beichman, C. A., Stapelfeldt, K. R., Hines & D. C. 2005, *ApJ*, 620, 1010
- Sackmann, I.-J., Boothroyd, A. I. & Kraemer, K. E. 1993 *ApJ*, 418, 457
- Santos, N. C., Israelian, G., Mayor, M., Bento, J. P., Almeida, P. C., Sousa, S. G., Ecuivillon, A. 2005, *A & A*, 437, 1127
- Sato, Bun'ei, Kambe, Eiji, Takeda, Yoichi, Izumiura, Hideyuki, Masuda, Seiji, Ando & Hiroyasu, 2005, *PASJ*, 57, 97
- Sato, B., Izumiura, H., Toyota, E., Kambe, E., Takeda, Y., Masuda, S., Omiya, M., Murata, D., Itoh, Y., Ando, H., Yoshida, M., Ikoma, M., Kokubo, E. & Ida, S., 2007, *ApJ*, 661, 527
- Schlaufman, K. C., Lin, D. N. C. & Ida, S. 2008, *arXiv*, 0809, 1651
- Siess, L. & Livio, M. 1999, *MNRAS*, 308, 1133
- Siess, L. & Livio, M. 1999, *MNRAS*, 304, 925
- Stern, S. A. 1996, *AJ*, 112, 1203
- Stern, S. A., Shull, J. M. & Brandt, J. C. 1990, *Natur*, 345, 305
- Stewart, S. T. & Leinhardt, Z. M. 2008, *LPI*, 39, 2207

- Su, K. Y. & Rieke, G. H. 2005, AAS, 210, 7506
- Su, K. Y. L., Chu, Y.-H., Rieke, G.H., Huggins, P.J., Gruendl, R., Napiwotzki, R., Rauch, T., Latter, W.B., & Volk, K., 2007, ApJ, 657L, 41
- Supulver, K. D. & Lin, D. N. C. 2000, Icar, 146, 525
- Tanaka, H. & Ida, S. 1996, Icar, 120, 371
- Trilling, D. E., Bryden, G., Beichman, C. A., Rieke, G. H., Su, K. Y. L., Stansberry, J. A., Blaylock, M., Stapelfeldt, K. R., Beeman, J. W., Haller, E. E. 2008, ApJ, 674, 1086
- Trujillo, C. A., Luu, J. X., Bosh, A. S. & Elliot, J. L. 2001, AJ, 122, 2740
- Vidal-Madjar, A., Lacavelier des Etangs, A., Desert, J.-M., Ballester, G.E., Ferlet, R., Hebrard, G., & Mayor, M., 2003, Nature, 422, 143
- Weidenschilling, S. J. 2004, STIN, 0523594
- Williams, D. R. & Wetherill, G. W. 1994, Icar, 107, 117
- Willson, L. A. 2000, ARA&A, 38, 573
- Wyatt, M.C. Dermott, S.F., Telesco, C.M., Fisher, R.S., Gorgan, K., Holmes, E.K., & Pina, R.K., 1999, ApJ, 527, 918
- Wyatt, M.C. Smith, R., Greaves, J.S., Beichman, C.A., Bryden, G. & Lisse, C.M., 2007, ApJ, 658, 569
- Youdin, A. & Chiang, E. 2004, ApJ, 601, 1109
- Zhou, J.-L. & Lin, D. N. C. 2007, ApJ, 666, 423



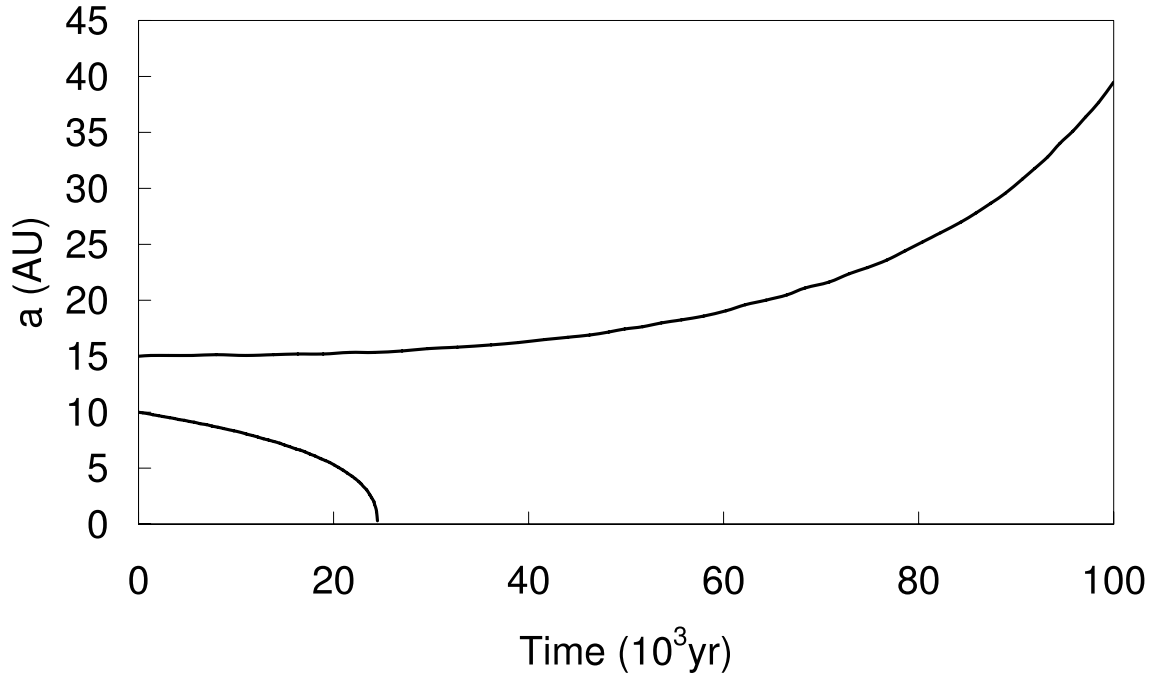


Fig. 1.— Orbital evolution of two planetesimals around a mass-losing star. The initial mass of the central star in this simulation is  $4 M_{\odot}$ . It loses 75% of its mass at a constant mass loss rate over  $10^5$  years (from now on it is called "linear mass loss"). The upper and lower curves in the plot show the evolution of semi-major axis verse time of two identical planetesimal, with density  $\rho = 3 \text{ g/cm}^3$  and size  $s = 1 \text{ km}$ . The upper one starts from 15 AU, and its size is larger than the  $s_c$  at that position, so its orbit expands. While the lower one starts from 10 AU, with its size being smaller than  $s_c$  at that position, it undergoes orbital decay, and finally drops into the star within about 25,000 years.

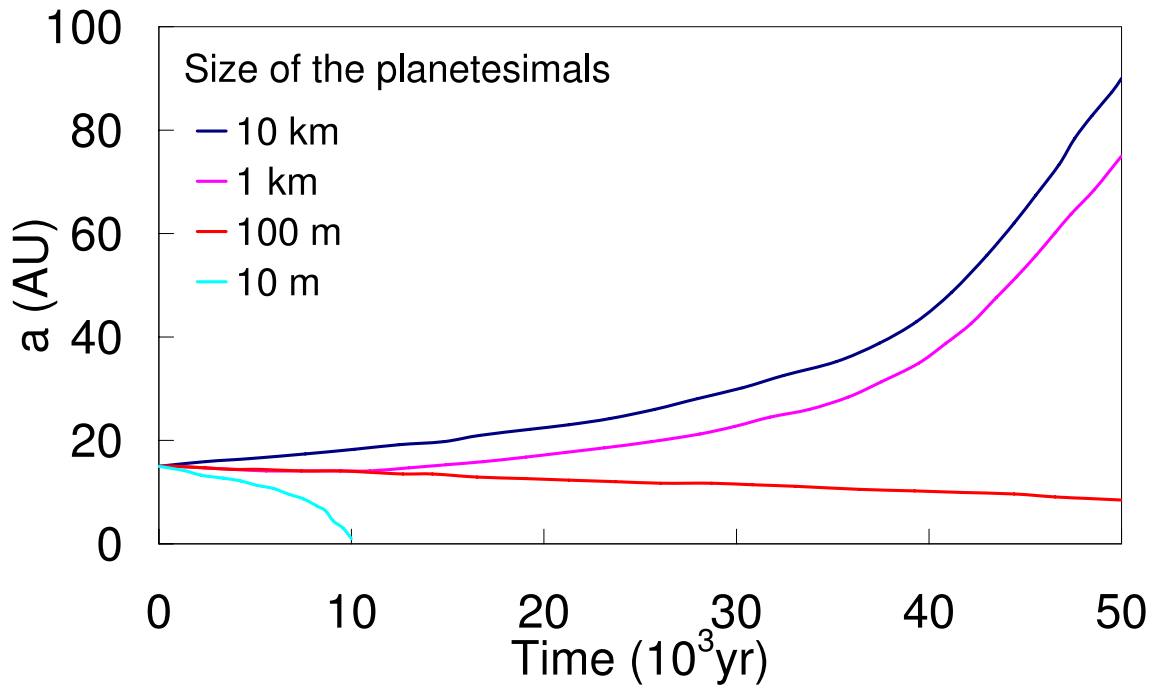


Fig. 2.— Orbital evolution of 4 planetesimals. The mass of the star changes linearly from an initial value  $M_i = 3 M_\odot$  to a final value  $M_f = 0.5 M_\odot$  in 50,000 years. Curves show the evolution of semi-major axis as a function of time for 4 objects all starting from 15 AU, with size  $s =$  (from top to bottom) 10 km, 1 km, 100 m and 10 m. The wind velocity is  $v_{wind} = 10 \text{ km s}^{-1}$

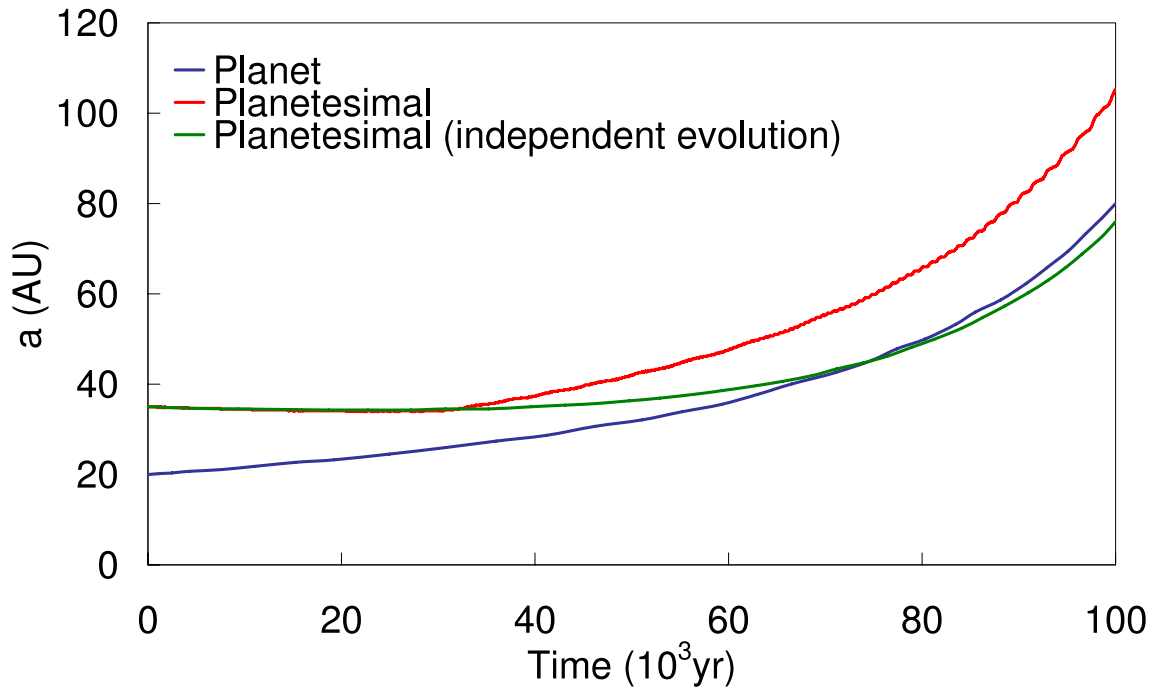


Fig. 3.— This plot compares the orbital evolution of a  $s = 0.1$  km planetesimal when there is a giant planet in the system (red) or not (green), while the blue curve shows the orbital evolution of the planet. The density of the planetesimal is  $\rho_p = 3 \text{ g cm}^{-3}$  and it starts out with a circular orbit at 35 AU around a  $M_i = 4 M_\odot$  star which linearly reduces its mass to  $M_f = 1 M_\odot$  on a time scale of 100,000 yr through a wind with a speed  $v_{wind} = 10 \text{ km s}^{-1}$ . The planet with a mass  $M_p = 1 M_J$  was placed in a circular orbit at 20 AU initially.

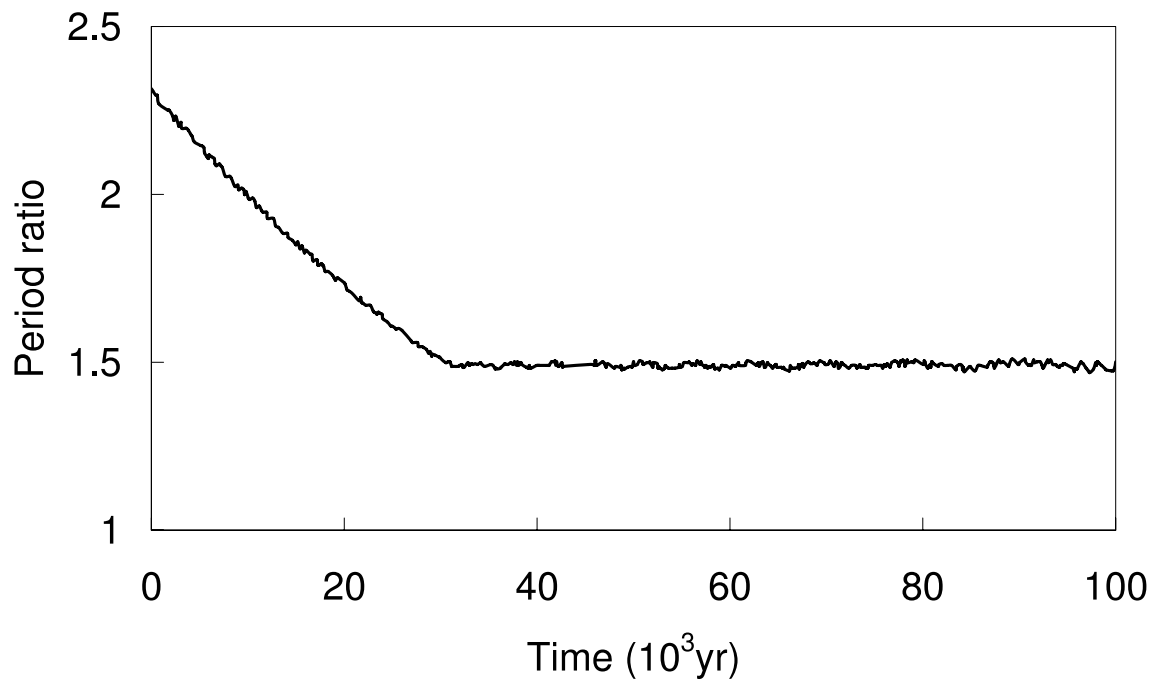


Fig. 4.— The evolution of period ratio ( $\frac{P_{\text{planetsimal}}}{P_{\text{planet}}}$ ) verse time for the system in Figure 3.

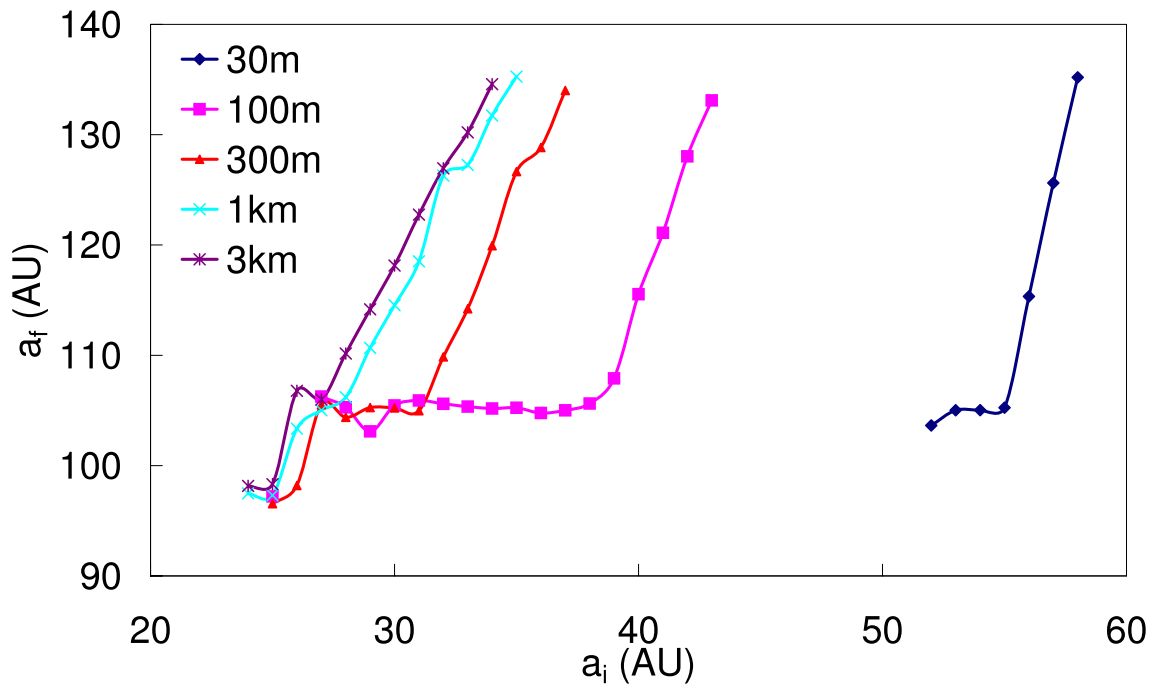


Fig. 5.— The orbital evolution of a group of different-size planetesimals verse time. The size of the planetesimals in the five curves are (from left to right) 3 km, 1 km, 300 m, 100 m and 30 m. The system is the one in Figure 3.

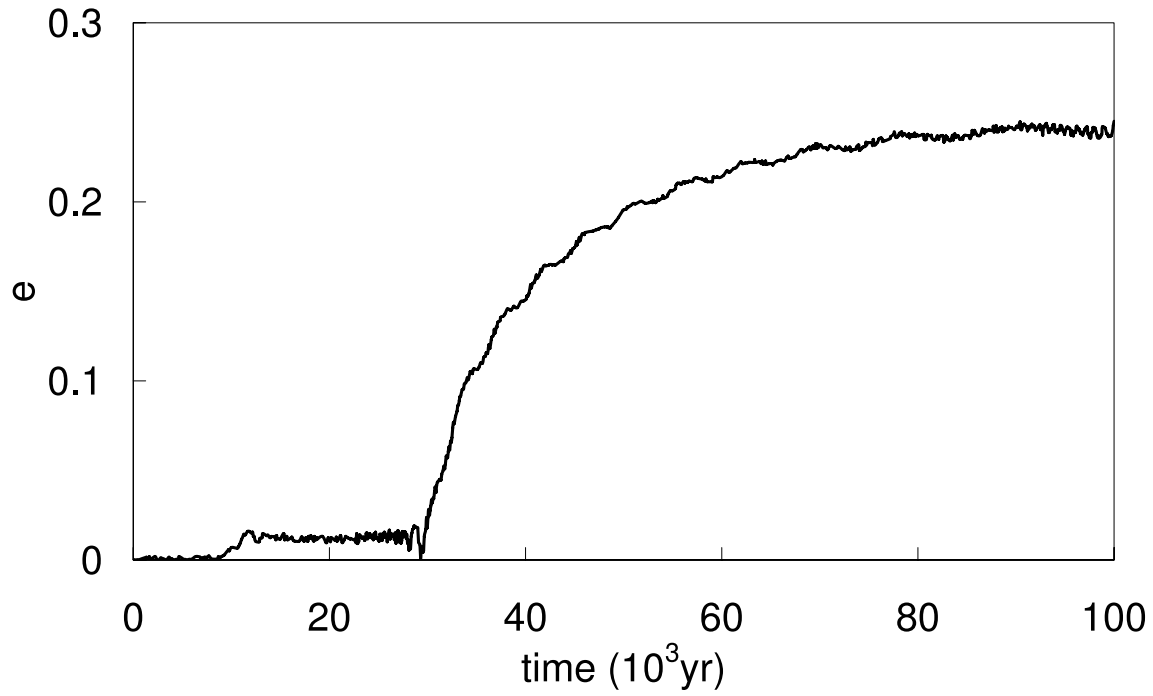


Fig. 6.— The eccentricity evolution of the 100m-size planetesimal in the system of Figure 3

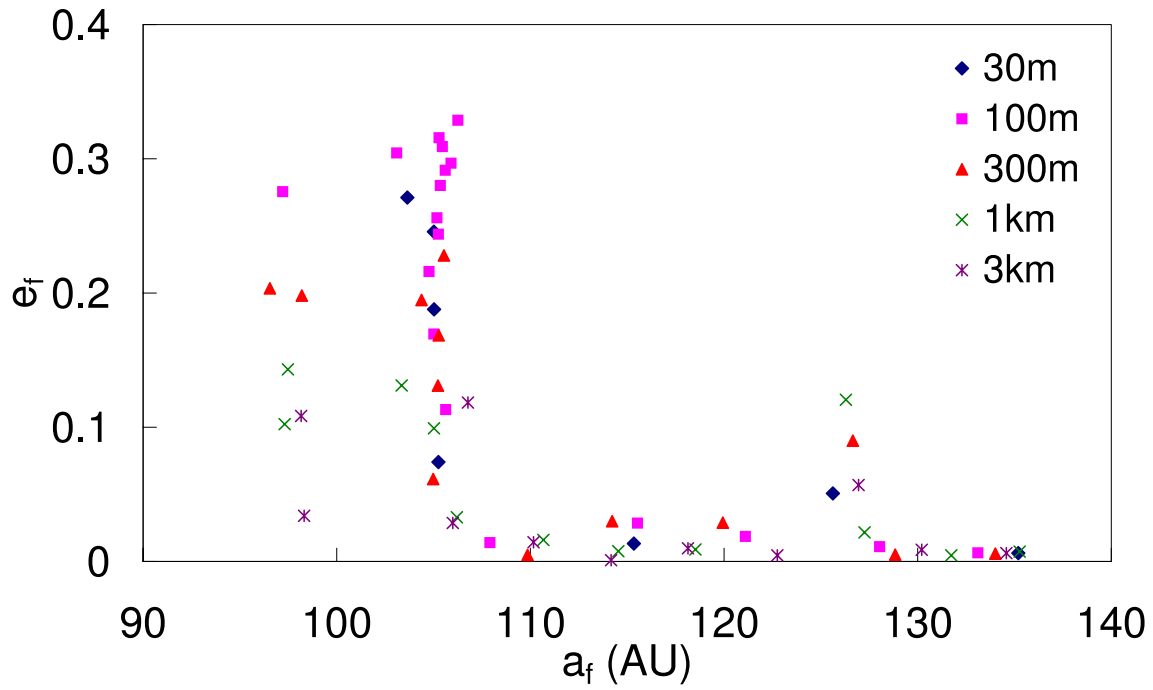


Fig. 7.— The final eccentricity verse final semi-major axis for several planetesimals with different sizes in the system of Figure 5.